POLITECNICO DI MILANO
Scuola di Ingegneria dei Processi Industriali
Corso di Laurea Specialistica in Ingegneria Nucleare
Dipartimento di Energia

GEL DOSIMETRY METHODS FOR DOSE MEASUREMENTS IN SMALL PHANTOMS IRRADIATED AT NCT EPITHERMAL COLUMN

Relatore: Fabrizio Campi
Correlatore esterno: Grazia Gambarini

Tesi di Laurea di:
Raffaele Nolli
Matr. Nr. 751615

Anno Accademico 2011-2012

Contents

List of Figures

List of Tables

Abstract

In this work the possibility of developing gel dosimetry methods for BNCT in small phantoms has been analysed. Boron Neutron Capture Therapy is an experimental radiotherapy that exploits the high cross section of ^{10}B for neutron capture, to selectively target cancer cells. This work concerns the development of gel dosimeters based on Fricke solution, with the addition of Xylenol orange colouring agent; Fricke gel dosimeters can provide images of the spatial dose distributions of the different dose components absorbed in a tissue equivalent phantom, subject to an epithermal beam. Dose component separation can be achieved using dosimeters of different isotopic composition. In this work Boron an Gamma dose separation was performed using borated gel dosimeters, while fast neutron dose was taken into account. Production and analysis methods of small dosimeters in form of thin cylinders (straws) and cuvettes are described; such dosimeters were developed to investigate dose distributions in small targets. The analysis is carried out by acquiring with a CCD camera optical transmittance images, at the suitable wave-lenght, of dosimeters placed on a LED plain light source. By pixel-to-pixel manipulation of the images, it is possible to obtain images of the difference of optical density (ODD), which is proportional to the absorbed dose. Dose profiles and averaged values were obtained analytically with cuvettes; straws, due to their limited diameter (3 mm), required a dedicated Matlab code able to find their transmittance peak from pictures. Dosimeters characterization was carried out, including linearity and saturation studies, calibration, cooling uniformities and evaluation of gel performances stability over time. The results obtained at the BNCT facility of LVR-15 reactor in Řež(CZ) are presented. The experimental campaign was performed in support of BNCT studies on biological targets. The irradiation ge-

ometry was reproduced, and dose profiles in mice and cell cultures phantoms were obtained. Emphasis has been given to the irradiation geometry impact on dose distributions, in particular of the size of phantoms made of moderating tissue equivalent materials, and beam geometry.

Abstract (Italiano)

In questo lavoro si è analizzata la possibilità di sviluppare dosimetri a gel per BNCT per piccoli fantocci. La terapia a cattura neutronica del boro è una tecnica sperimentale che sfrutta l'alta sezione d'urto del ^{10}B di cattura neutronica per colpire selettivamente le cellule tumorali. Questo lavoro concerne lo sviluppo di dosimetri basati sulla soluzione di Fricke, con l'aggiunta del colorante Xylenol Orange;i dosimetri a gel di Fricke possono fornire immagini di distribuzioni spaziali di dose delle diverse componenti di dose assorbita in fantocci tessuto equivalenti, irraggiati con fascio epitermico. La separazione delle componenti può essere effettuata con dosimetri di diversa composizione isotopica. In questo lavoro si è effettuata la separazione delle dosi Gamma e da boro, e si è valutata la dose da neutroni veloci. Si è descritta la produzione e analisi di dosimetri sotto forma di cannucce sottili e cuvette, adatti a investigare dosi in piccoli oggetti. L'analisi è compiuta acquisendo con una camera CCD immagini di trasmittanza ottica, ad una opportuna lunghezza d'onda, dei dosimetri posti su un illuminatore LED. Con l'analisi pixel a pixel delle immagini si possono ottenere immagini di differenza di densità ottica (ODD), che è proporzionale alla dose assorbita. Profili di dose e valori mediati si sono ottenuti dalle cuvette analiticamente;le cannucce, a causa del diametro limitato (3 mm), hanno richiesto lo sviluppo di un codice Matlab per individuare il loro picco di trasmittanza dalle immagini. Si sono caratterizzati vari aspetti dei dosimetri, come la linearità, saturazione, calibrazione, disuniformità di raffreddamento e stabilità nel tempo delle performance del gel. Si riportano i risultati ottenuti presso il reattore LVR-15 a Řež(CZ). La campagna di esperimenti si è svolta a supporto di studi di BNCT su campioni biologici. Si è replicata la geometria di irraggiamento, ricavando profili di dose in fantocci di piccoli topi e

culture cellulari. Si è inoltre considerato l'impatto sulle distribuzioni di dose della geometria del fascio e della dimensione dei campioni, in particolare per la moderazione dei materiali tessuto equivalenti.

Chapter 1

Boron Neutron Capture Therapy

1.1 Principles

Boron Neutron Capture Therapy (BNCT) is an experimental technique based on the nuclear reaction occurring when boron-10 (^{10}B) is irradiated with thermal neutrons to split into high linear energy transfer (LET) α particles and lithium-7 (^{7}L) nuclei. The reaction has a very high cross section (σ = 3837 b) at thermal energies and is schematized in figure :

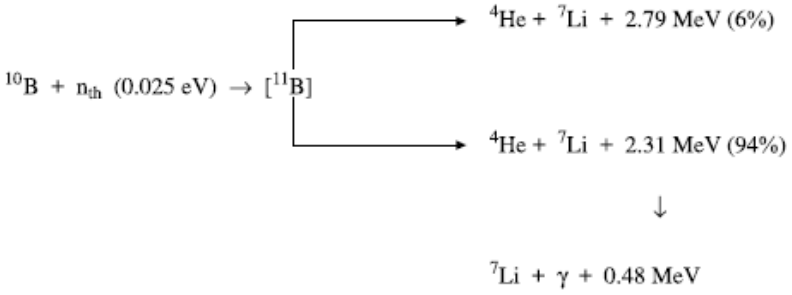

Figure 1.1: Boron-10 fission reaction occurring after neutron capture

The aim of the technique is to fixate a ^{10}B containing carrier into the tumor cells: the range of the reaction products is comparable to cell dimensions, hence selectively destroying them without severely affecting the adjacent healthy tissue. Clinical applications mainly focused on the treatment of tumors that

are highly resistant to all current forms of therapy, such as glioblastoma multiforme, melanoma metastases, and more recently head and neck and liver cancer; all of these diseases are characterized by a strong radioresistance and by their spreading of microinvasive tumor cells within the brain or liver tissue which conventional therapies are uneffective to eradicate.
The major challenge facing the BNCT research is to find a boron carrier with a few important requirements:

- Low toxicity and selectively targeting malignant cells in complex environments such as the brain tissue, thus ensuring a high tumor/brain and tumor/blood ratios (3-4:1 at least).
- Persistence in tumor for an adequate time during BNCT.
- Tumor concentrations of $\sim 35\mu$g of $^{10}\mathbf{B}$/g tumor

At the moment several kinds of boron carriers have been studied, none fulfils these criteria yet, although combinations of agents with different properties (size, solubility, lipophilicity...) seem to be more effective [1], and new and more effective carriers are being researched.

1.2 Neutron Sources for BNCT

Neutron sources for BNCT are currently limited to nuclear reactors, and even though particle accelerators could be used to enhance a neutron producing nuclear reaction, reactors are the only sources able to achieve the necessary therapy fluency ($5 \times 10^{12}\text{cm}^{-2}$ per hour).
Neutrons are divided in three classes according to their energy:

- thermal ($E_n < 0.5$ eV)
- epithermal (0.5 eV $< E_n < 10$ keV)
- fast ($E_n > 10$ keV)

Even though thermal neutrons are the most important to trigger the ^{10}B reaction, their limited depth of penetration makes them unsuitable for tumors well

below the surface; epithermal neutrons are then preferred for clinical therapy since they lose energy and become thermal as they penetrate tissues. Thermal beams remain the best solution for surface treatments such as melanoma or glioma treatments with open craniotomy.
Figure 2.2 shows the trend of thermal neutron flux for thermal and epithermal beams.

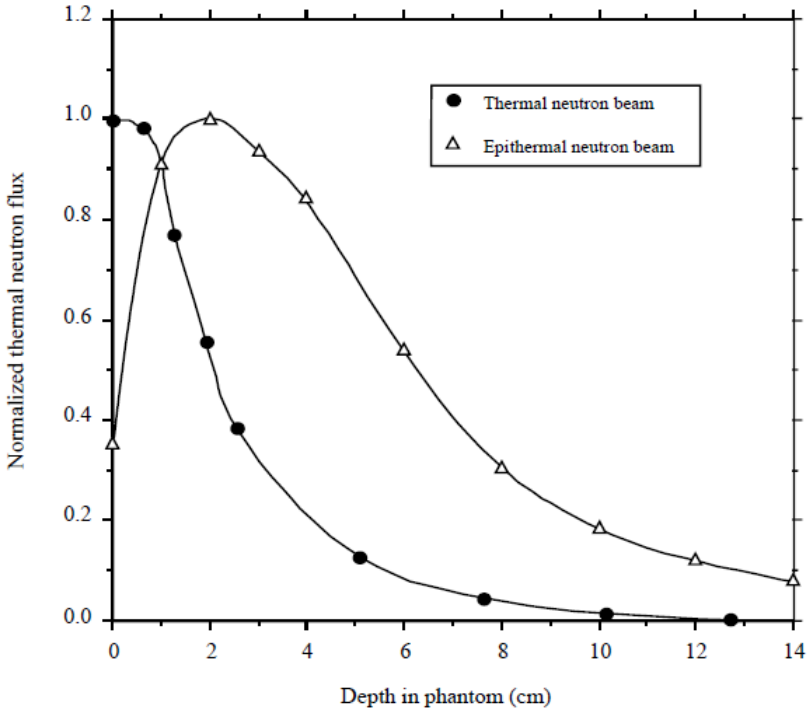

Figure 1.2: Comparison of in-depth thermal flux distributions for thermal and epithermal neutrons.

Extensive reports have been written with the purpose to study and set general standards about desired beam parameters and quality [2] [3]. General desirable beam properties can be summarised as:

- minimum beam intensity of 10^9 epithermal neutrons $cm^{-2}s^{-1}$. Lower intensities often results in unacceptable longer irradiation times, while higher intensities usually mean worse beam quality.

- the fast neutron component should be kept as lower as possible, since

it causes a collateral non-selective dose from high LET recoil protons. A target value for the dose of this component should be 2×10^{-13}Gy cm^2 per epithermal neutron.

- the gamma ray component should be kept as lower as possible as well, since it results in an non-selective dose to both tumour and healthy tissue. A target value for the dose of this component should be 2×10^{-13}Gy cm^2 per epithermal neutron.

- the thermal component results in an additional damage to the scalp; the ratio of thermal flux to epithermal flux should be around 0.05.

- the ratio of total neutron current to total neutron flux measures the general collimation of the beam. A high value means a little beam divergence and a lesser collateral dose to tumour-adjacent tissues, and more flexibility in patient positioning.

- the beam size should be set in accordance with the tumour size. Currently circular apertures of 12 to 14 cm are being used being studied for head treatments, while larger sizes have been proposed for trunk treatments.

As said before, the only available neutron sources are research reactors, mostly thermal. It is necessary to moderate the out-coming neutron flux to make it suitable for BNCT. The two basic methods to customize the beam are termed *spectrum shifting* and *filtering* .
Spectrum shifting is usually used when a reactor has a large aperture such as an irradiation column; it consists in moderating the flux to an appropriate lower energy (thermal or epithermal), possibly in combination with a filter. Filtering is used when a long and narrow beam is available, and it transmits neutrons of the desired energy while blocking those of other energies. The Shifting technique gives a higher flux-to-power ratio; in current facilities a combination of the two techniques is mostly used in order to optimize such factor. A third alternative technique is to use fission converters such as nuclear fuel elements in the beam line generating a beam of fast neutrons which can be moderated and

filtered giving a high intensity flux close to the treatment position.
If the possibility of a reactor designed specifically for BNCT was possible, a fast reactor would be preferred. Such a facility could be very efficient at low power and provide a higher comfort to patients. Even though designing a very safe and efficient reactor for BNCT is very feasible, public acceptance would still be a major problem.
Particle accelerators would be the ideal solution for a hospital, since they involve fewer technical and bureaucratic problems, and also public acceptance would not be an issue. An ideal treatment room could easily incorporate the instrumentation for real time determination of boron concentration in blood. However, this technology is not yet available, since it has not been possible yet to achieve the required beam intensities. A facility is being completed in Japan where a liquid lithium self-cooling flow is to be used as target for a proton beam, seeming to elude most of the excessive heating problems connected to solid targets.

1.3 Dosimetry for BNCT

1.3.1 Principles of Dosimetry

Dosimetry is the branch of physics that studies the energy absorption of matter under radiation exposure, with particular focus on ionizing radiation in medical dosimetry: exposition to ionizing radiation leads to damages to biological systems proportionally to the entity of exposition. In medical physics, radiation has mainly two uses: radiotherapy and radio-diagnostics. In radiotherapy, high doses are concentrated on small volumes such as tumors, while in radiodiagnostics X-rays or radio-isotopes tracers are used to gather physiological or functional informations about biological systems. In either case high precision is required to ensure therapy's effectiveness and low doses to healthy tissues, and the purpose of dosimetry is then to ensure such precision. ICRU 51 defines the absorbed dose D as:

$$D = \frac{d\bar{\varepsilon}}{dm} \tag{1.1}$$

where $d\bar{\varepsilon}$ is the mean energy deposited by ionizing radiation in an infinitesimal portion of mass dm. D depends on the type of radiation, its flux and by the medium itself. The mass portion dm and the corresponding volume portion dV are small relatively to macroscopic dimensions, but big enough to let the concept of mean energy release maintain sense. As long as dV is large compared to interaction typical scales, D remains constant among adjacent dV portions. But as dV becomes smaller, at a certain scale D will show large discontinuities due to the discrete nature of interactions, and the concept of dose as an averaged quantity is no longer useful. The study of microscopic energy release is called Microdosimetry.
The absorbed dose is a non-stochastic quantity and is measured in Gray [Gy], defined as Joule per kilogram [J/kg]. One of the critical issues of BNCT, alongside with Boron carrier development, is the estimation of the treatment dose delivered to the tumour and to nearby healthy tissue. Three aspects of the problem must be considered:

- the neutron beam is composed by different kinds of radiation, each giving its own dose distribution and behaving differently with respect to the geometry of the target.
- the target geometry is of major importance to estimate the thermal and epithermal neutron distribution.

In contrast with conventional radiotherapy, each component of the radiation field has to be quantified separately considering the different biological weighting factor;
It is also necessary to characterize the neutron beam spectrum and spatial distribution with in-air and in-phantom measurements, where in-phantom measurements are necessary to estimate dose in tissues.

1.3.2 Dose components in BNCT

Given a reactor-generated radiation beam consisting of neutrons and photons, four dose components are produced as it enters biological tissue:

1. the gamma dose, induced in the tissue itself, i.e. by the thermal neutron induced reaction ^{1}H(n,γ)^{2}H which generates 2.2 MeV gamma rays, or due to the gamma rays accompanying the beam.

2. The fast and epithermal neutron dose, which generates mainly recoil protons, a high LET radiation component.

3. The proton dose from nitrogen capture, due to the thermal neutron induced reaction ^{14}C(n,p)^{14}N, which produces a 600 keV proton and a recoiling ^{14}N nucleus.

4. The radio-therapeutic dose due to the ^{10}B fission reaction (see figure 2.1).

Fast neutrons and gamma radiation can be measured both in-air and in-phantom. In-air measurements are useful for general characterization of epithermal neutron beams, whereas in-phantom measurements (with computational simulations) are necessary for treatment planning. kerma approach[4].

1.3.3 Relative Biological Effectiveness (RBE) and Compound Biological Effectiveness (CBE)

RBE of a radiation source is defined as the ratio of doses of a reference gamma radiation, currently cobalt-60, to the test radiation producing the same biological effects in a given system. The RBE is a function of the radiation LET and is extremely variable depending on dose levels, biological tissue, dose rate and fractionation, experimental conditions. Though very difficult to determine experimentally, tabulated values for healthy tissue are available.
BNCT however is characterised by an inhomogeneous dose distribution, therefore the concept average absorbed dose, quantity with respect of which the RBE is calculated, cannot be applied. This is caused by the selective Boron carrier

distribution and the short range of the α and lithium particles; only a combination of this factors can be calculated, and it is referred to as Compound Biological Effectiveness (CBE) or Compound Factor.
Other factors are to be taken into consideration; e.g. irradiation times are determined by the dose rate, which is himself determined by the Boron carrier concentration dynamics and the neutron flux. During protracted or fractioned irradiation, damage from low-LET gamma radiation may undergo repair and thus a Dose Reduction Factor (DRF-γ) is to be considered.

1.3.4 Considerations about Irradiation Geometry and Dose Measurement Uncertainties

The measurements of dose distributions within the target, the adjacent body parts and in the whole treatment room, is a necessary step in BNCT dosimetry. Spatial measurements with standard detectors such as Bonner spheres, thermoluminescence detectors or activation foils are usually utilised for the characterization of the radiation field which is essential for treatment and collateral patient dose calculation during the treatment planning process.
These methods are though useful to estimate dose distributions interpolating a finite number of punctual measurements; an experimental method based on gel dosimeters in form of layers has been proposed and developed [5]. Using these dosimeters, based on Fricke solution, it is possible to obtain images of boron, gamma and fast neutron dose, with the immediate advantage of obtaining continuous dose distributions with one measure. Over the years dosimeter of different dimensions have been used, measuring dose distributions in water and gel phantoms of various sizes. The size of water or gel phantoms has a great impact on measured dose distribution, as the surrounding moderating volume deeply affects boron and gamma dose. In fact as the epithermal beam penetrates, neutron thermalise and their isotropy increase. They can thus be subject to backscattering towards the collimator. Mean free path of neutrons in air is much longer than in moderator, thus backscattering is much less probable in air. Thermal neutron flux is then lower in small phantoms, in any position. This

affects also gamma dose distribution, since its major contribution comes from the reaction ^{1}H(n,γ)^{2}H which generates 2.2 MeV gamma rays. The boron dose distribution therefore represents a distribution of gamma sources, and gamma dose will increase with the irradiated volume.
A few other possible effects can occur:

- Scattering and epithermal neutron moderation: small structural objects, containers etc. can affect the neutron flux distribution by altering its uniformity.
- Activation of materials: plastics, glues, coloured ink or tissue etc can be subject to activation, often in an unpredicted way.
- Shielding: the effectiveness of materials used as shields (Boron, Cadmium etc.) is very difficult to quantitatively estimate.
- Flux depression: big volumes with high Boron concentration can affect the flux distribution.

All of these effects affect every irradiation set-up in a unique and sometimes unpredicted way. As it is shown in the sixth chapter, approximated measures of dose profiles can be carried out with gel dosimeters replicating the irradiation set-up, allowing post hoc considerations about the biological effects observed on the treated subjects.

Chapter 2

The LVR-15 Research Reactor in Řež

2.1 Reactor Characteristics

The LVR-15 Reactor was commissioned in 1957 and has undergone reconstruction several times, the last one in 1989 by Skoda company. The LVR is a tank type light water reactor using fuel with 36% (currently) and 20 % (proposed) of enrichment. The theoretical maximum achievable power is around 18 MW, while at the moment it is limited to 10 MW, partly because of the limited heat exchange capacity of the fuel. The reactor duty cycle is 21 days, with 8-10 cycles per year. The simplified reactor structure is shown in figure 3.1, while figure 3.2 shows an horizontal section of the core [7] [8].

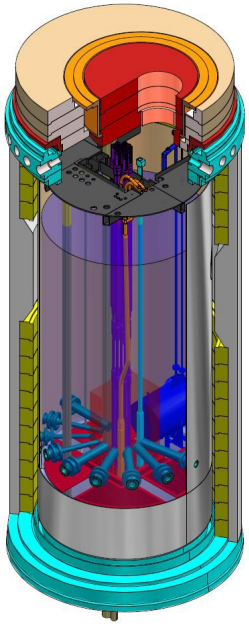

Figure 2.1: Simplified structure of the reactor

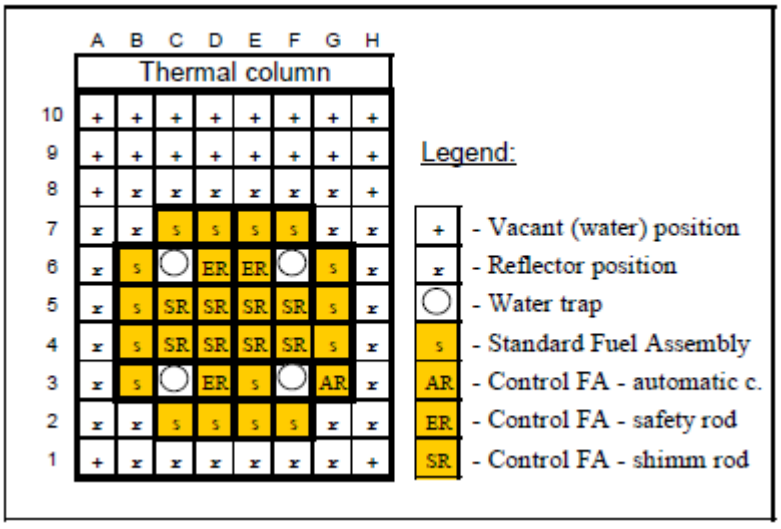

Figure 2.2: Typical configuration of the core

The core assembly is composed by concentric circles with the reflector surrounding the fuel rods and the control rods in the center. The reactor is a multipurpose facility, allowing research and services in many fields such as:

- Reactor technology studies: the reactor can simulate BWR(Boiling Water Reactor), PWR (Pressurized Water Reactor) and VVER(Water-Water Power Reactor in Russian) reactor environments by means of reactor water loops, to study ater chemistry, corrosion, physical and radiation stresses on materials.
- Production of radiation doped silicon.
- Activation analysis and material irradiation in rigs.
- Production of radio isotopes for radio pharmaceuticals and technical radiation sources
- BNCT and other neutron physics research at reactor horizontal channels.

The structure of the horizontal neutron beams is shown in figure.

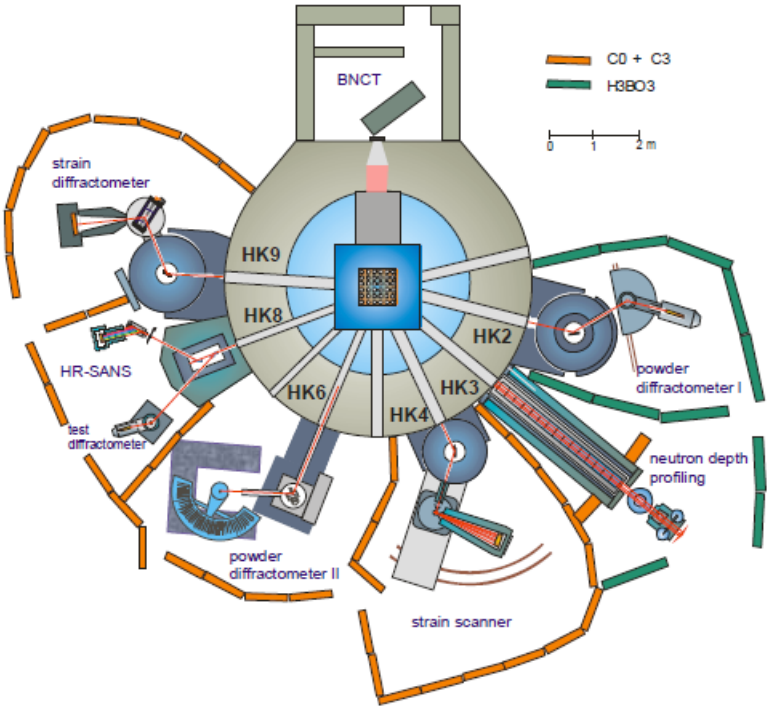

Figure 2.3: Horizontal neutron beam facilities

2.2 History of BNCT in Řež

First BNCT experimentations in Czech Republic were carried out from September 2000 to March 2002, after protocol approval by State Institute for Drug Control and State Office for Nuclear Safety. Nine patients with clinically diagnosed glioblastoma multiforme were included in the study: BSH boron carrier (Sodium mercaptoundecahydro-closo-dodecaborate) was infused in saline solution and its concentration was monitored in time in various tissues, thus estimating carrier concentration dynamics in time for each patient. Five out of nine patients were indicated for BNCT, the other being unsuitable due to insufficient Boron accumulation in tumor or different histology. The average ratio of ^{10}B concentration in tumor and healthy tissue was studied in time. The actual ratio was highly variable among patients and parts of tumor, and the ^{10}B skin concentration was often not negligible, leading to grade II skin reactions.
The study showed relatively good tolerance of the BNCT under the used conditions; the authors of the study [9] suggest further investigation with higher doses and a larger patient sampling .

2.3 The epithermal neutron beam at LVR-15

Neutrons generated in the reactor core are fast and randomly directed; for BNCT purposes beam has to be moderated so that most of them turn to epithermal energies, and collimated. The simplified beam structure is shown in figure.

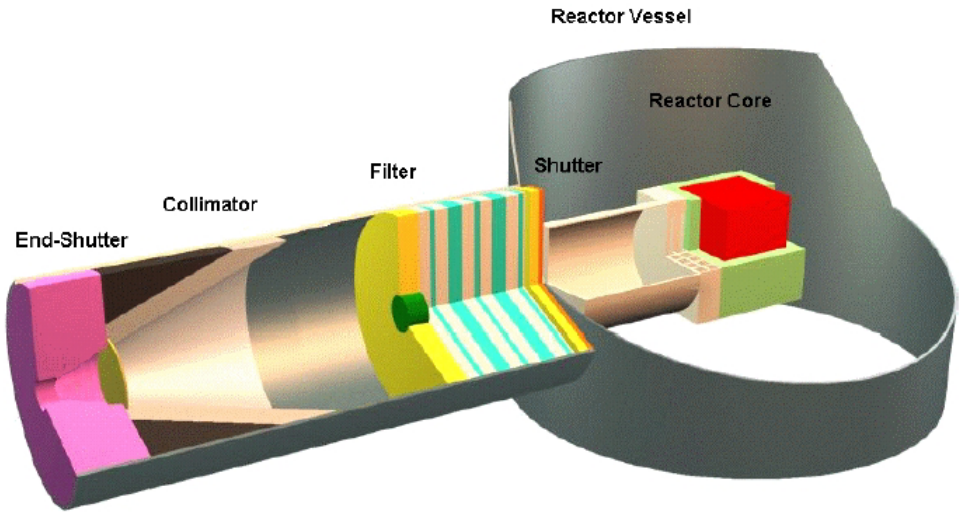

Figure 2.4: BNCT neutron beam on LVR-15 reactor

The epithermal neutron beam of the LVR-15 reactor has been characterized in previous works [11]. The beam spectrum has been calculated with Monte Carlo (MC) simulations supported by activation foil measurements. It should be noted that the fast component is not negligible.

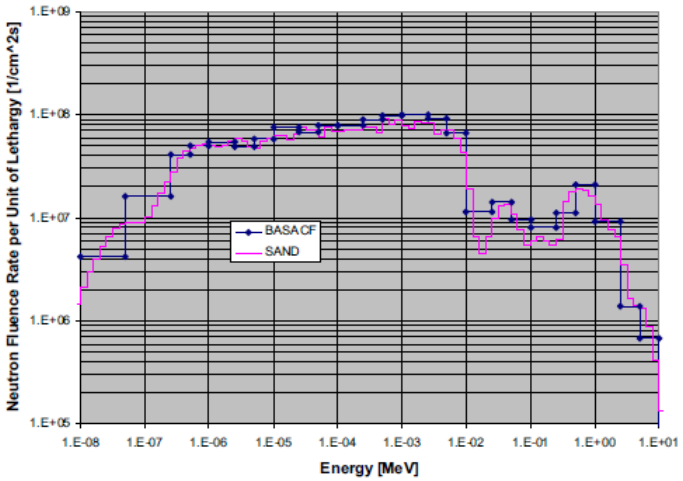

Figure 2.5: Neutron beam spectrum, calculated with MC simulations and activation foil measurements

Images of fast neutron and gamma dose at a distance of 1 cm from the collimator mouth edge have been obtained in a previous study by Gambarini et al.

[6] an are reported in figure.

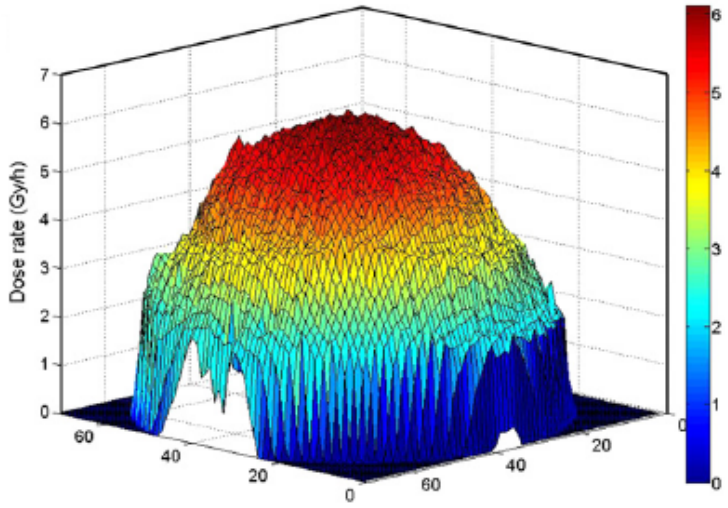

(a)

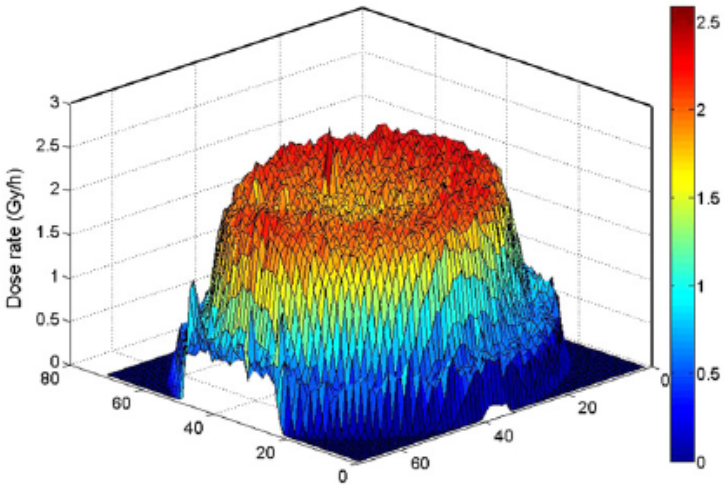

(b)

Figure 2.6: Images of spatial distribution of (a) fast neutron dose and (b) gamma dose, 1 cm from the collimator mouth edge

This profiles have been obtained by means of Fricke gel dosimeters in form of circular layers, with a diameter of 18 cm. Dosimeter were fixed 1 cm away form the beam mouth, without moderation. The experimental setup is shown in figure:

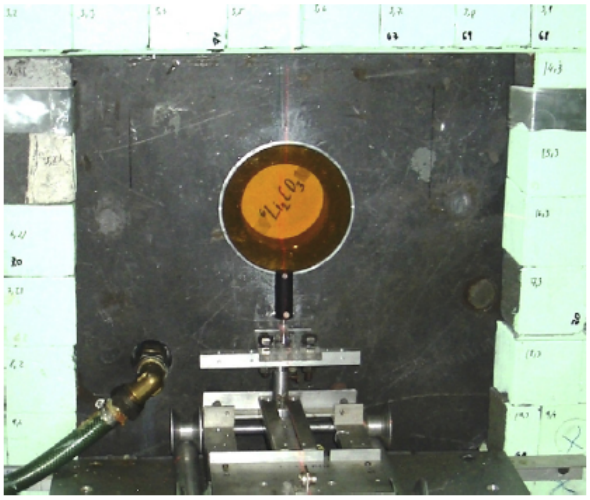

Figure 2.7: Fricke gel dosimeter against the LVR-15 epithermal column mouth

Results are consistent with previous measurements obtained by other techniques such as ionization chambers [10], but obtained with single irradiation of few dosimeters, instead of interpolation of point measurements.

Chapter 3

The FriXy Gel Dosimeter

3.1 Composition

The standard Fricke dosimeter is a liquid solution of ferrous ammonium sulphate in sulphuric acid, where the chemical species of interest is the Ferrous ion (Fe^{2+}), that through induced chemical reaction induced by radiations, is oxidised to Ferric ion (Fe^{3+}), with yield proportional to the adsorbed dose. Since the Ferrous ions in mM concentrations are in water solution, their contribution doesn't affect sensibly the absorbed dose, but they allow its measurement; Ferric ions are generated via interaction with radicals and ions produced from water:

$$H + O_2 \rightarrow HO_2$$
$$Fe^{2+} + HO_2 \rightarrow Fe^{3+} + HO_2^-$$
$$HO_2^- + H^+ \rightarrow H_2O_2$$
$$Fe^{2+} + H_2O_2 \rightarrow Fe^{3+} + OH + OH^-$$
$$Fe^{2+} + OH \rightarrow Fe^{3+} + OH^-$$

The FriXy gel dosimeter is a development of the standard Fricke dosimeter, stabilized in a gel matrix and with the Xylenol Orange colouring agent. Its composition has been studied and standardized [12]. In order to adapt this kind of dosimeter to neutron dosimetry we added a Boron compound to the Fricke solution, in our case Sodium Tetraborate Decahydrate [$B_4Na_2O_7 \bullet 10H_2O$], to obtain a desired concentration of 40 ppm of ^{10}B.

- Gelatine from Porcine Skin in powder
- Ferrous Sulphate solution [$Fe(NH_4)_2(SO_4)_2 \bullet 6H_2O$]
- Sulphuric Acid [H_2SO_4]
- Highly purified and deionized water
- Xylenol Orange [$C_{31}H_{28}N_2Na_4O_{13}S$]

The following table reports the concentrations of the chemical compounds:

Chemical Compound	**Concentration**
Gelatine	3% w/w
Ferrous sulphate solution	0.5 mM
Sulfuric acid	25 mM
Water	97% w/w
Xylenol Orange	0.165 mM
Sodium Tetraborate Decahydrate	0.49935 mM

Table 3.1: Composition of the Borated FriXy gel dosimeter

The presence of the Boron coumpound represents the difference between what we call *standard* and *borated* FriXy dosimeters.

3.2 Preparation of the Dosimeters

The gel dosimeter is prepared melting the gelling compound with the chemical compunds (Fricke solution), each part in half of the total amount of water. The Fricke solution has to be prepared taking care not to be shaken or mixed abruptly, since Oxygen incorporation would result in lower dosimetric performance. Once prepared, with or without Boron, it has to be kept away from light and possibly sealed. Gel is prepared mixing gelatin with water and heating the resulting solution for 20 minutes at 45°C, being continuously stirred (e.g. with a magnetic stirrer); once the 20 minutes have passed, the gel solution has to rest at room temperature until it reaches 35°C, and then the Fricke solution may be slowly poured into the gel, avoid air incorporation. Waiting the gel solution to cool down to 35°C is important, mainly because the sensitivity of the

dosimeter is sensibly dependent on cooling rate of the final solution. Since our study had to focus on dosimetry in small targets, such as cell culture flasks and mice phantoms, for our studies we used two different kind of dosimeters, little catheters (*straws*) and *cuvettes*. It was obviously was not possible to use layer dosimeters previously developed in the laboratory.

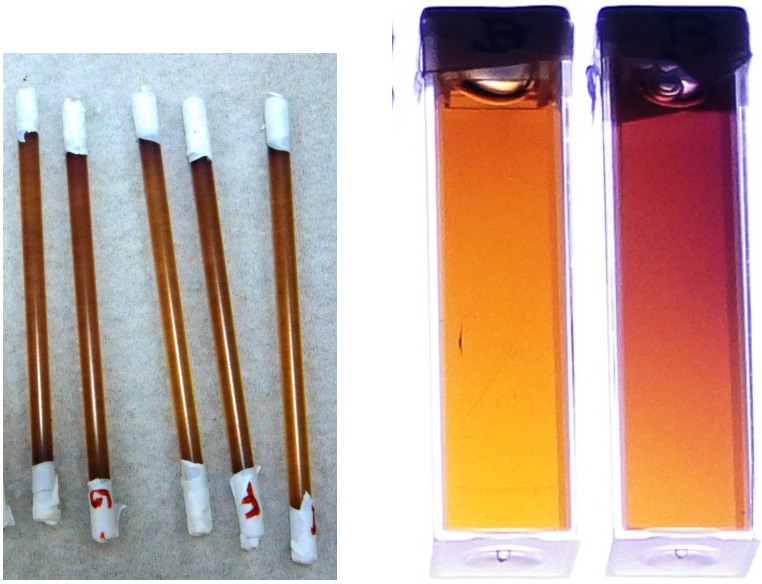

(a) (b)

Figure 3.1: Picture of straw (a) and cuvette (b) dosimeters.

Straws are thin rigid plastic cylinders 13 cm long, with an external diameter of 2.8 mm, and an internal diameter of about 2.2 mm. Their transparency and the quality of plastic ensures good optical quality, even after bending or cutting, an important characteristics being the analysis optical, as described in the following section. As a matter of fact, this kind of straws are commonly used in analysis of bovine semen. They can be easily cut without affecting their integrity, and their length was customized whenever necessary. For example in Řež it was necessary to cut them about 7 cm long, so that they could fit into mice phantoms. Because of their geometry, a filling method to avoid bubble formation is suction with a syringe. Straws cannot be filled with gel through injection; gel injection via syringe would lead to bubbles generation and gel could

easily fall out the open ending, being liquid after its preparation. Once filled with gel, their endings are sealed by mastic and Teflon tape. The straws we had were purchased from IMV Technologies Italia s.r.l., a company specialised in Biotechnologies and Veterinary products.
Cuvettes are the standard containers for photospectrometres, with external dimensions of 4.5cm ×1.2cm×1.2cm. Of the few types available, we used cuvettes with square section, with 4 or 2 transparent sides, and 1 cm of optical path. Of course it is important not to mix the two types of cuvettes in the same set, since optical analysis may not be equivalent. Once filled with gel, their caps were sealed with Teflon tape. With dosimeters realised in straws, it is possible to obtain dose profiles along the straw length, and with cuvettes it is possible to obtain informations averaged over the 1 cm of optical path.

3.3 Optical Analysis

Xylenol Orange (X.O.) is added to the solution compounds, as suggested by Appleby [13], because it forms a complex with the Ferric ion. The molecule X.O. absorbs light around 430 nm; the Fe^{3+}-X.O. complex absorbs light around 585 nm . This leads to a very efficient optical analysis of the dosimeters. Gel dosimeters prepared with Xylenol Orange are radiochromic, shifting their color from orange to purple through irradiation. The absorbed dose is proportional to the Optical Density Difference (ODD), deduced from light transmittance around ~585 nm detected with a CCD camera before and after irradiation [14].
After the irradiation, at least 40 minutes have to pass before the image acquiring. This time is necessary for the dosimeters to achieve chemical stability. Waiting long times to perform the image acquisition should be avoided, since the ions contained in the gel matrix, produced in the irradiation, incur in diffusion.
The optical density of a material traversed by light at a given wavelength can be defined as:

$$OD = \log_{10}(I_0/I) \tag{3.1}$$

Where I_0 is the intensity of the light entering the sample and I the transmitted light intensity, and their ratio I/I_0 is defined as *transmittance*. According to the Lambert-Beer law, if the analysed material contains an absorbing substance with absorption cross section for the considered wavelength σ, the OD can be defined as:

$$OD = n\,l\,\sigma \tag{3.2}$$

Where n is the absorber concentration and l the optical path length. From the previous equations, it is possible to express the transmitted light intensity with the following relation:

$$I = I_0 \exp(-n\,l\,\sigma) \tag{3.3}$$

Where the transmitted light is related to the absorber concentration.
The analysis setup is composed of a 25 cm × 25 cm plain uniform light source and a CCD camera, equipped with an optical filter (centered at 580 nm) and connected with a computer. The light source is covered with a black paper template, shaped to prevent any light to pass, apart through dosimeters and a grey scale strip, as shown in figure 3.2. The CCD camera used is an IDS uEye camera equipped with a 12.5-75 mm zoom lens (8 bit). The camera is controlled by a dedicated software that controls its settings, and allows images acquisition. This system was set to give greyscaled photos with a resolution of 768×582 pixels , where every pixel has its own grey level value from 0 to 255 (256 shades of grey). Gel dosimeters are therefore imaged as bidimensional matrices of grey level (GL) indexes. GL and intensity can be linearly related: the transmittance of an imaged dosimeter can be expressed as:

$$T = \frac{I}{I_0} = \left(\frac{GL}{255}\right) \tag{3.4}$$

being 255 the grey lever corresponding to white. If GL_b and GL_a are the grey-level matrices acquired before and after irradiation, the difference of optical density (ODD) induced by radiation in the dosimeter can be expressed as:

$$ODD = OD_a - OD_b = \log\left(\frac{I_0 I_b}{I_a I_0}\right) = \log\left(\frac{I_b}{I_a}\right) = \log\left(\frac{GL_b}{GL_a}\right) \tag{3.5}$$

where it is necessary that images before and after irradiation are taken with the same camera configuration for the equation to be true. From 3.2 comes that ODD is proportional to the variation of the absorber concentration, and that it can be quantified by pixel-to-pixel manipulation. The ODD measurement at around 585 nm therefore is proportional to the Fe^{3+}-X.O. complex variation in concentration. The yield of ferric ions, up to saturation effects, is proportional to the absorbed dose, therefore for each pixel applies:

$$\mathrm{ODD} = k \bullet \mathrm{D} \tag{3.6}$$

that is, the absorbed dose is linearly correlated to the obtained ODD matrix. The average ODD value over the whole dosimeter gives an information about the average absorbed dose in case of uniform irradiation, while pixel-to-pixel analysis can provide images of spatial dose distribution. The sensitivity coefficient k depends on gel composition and on the cooling rate during the gelling procedure: it is therefore affected by intrinsic uncertainties during the preparation process.

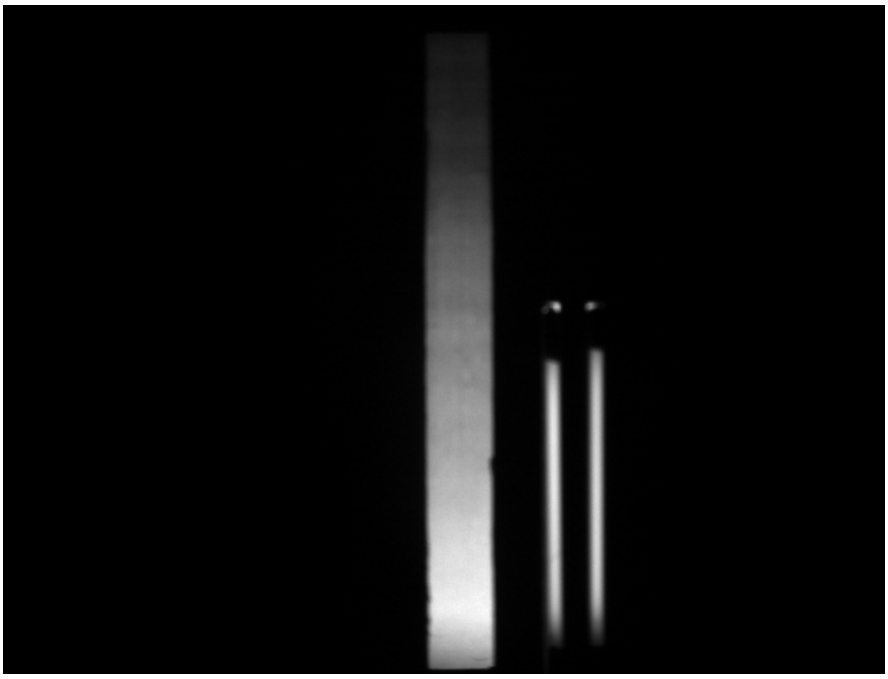

Figure 3.2: Example of greyscaled picture used for optical analysis

The grey level strip on the left is used as reference mainly in two situations:

- Extending the linearity range: changing camera parameters exposure time can avoid GL saturation occurring at high doses.
- Amending fluctuation in network voltage: even slight fluctuations can result in high distortions of ODD.

In either case, the evaluation of the variation of GL values of the reference strip in the images is necessary to control and eventually correct the obtained ODD values. It is also possible to acquire the images with two different exposure times: *t'*, used for the image before irradiation, and *t"*, used for the image after irradiation. The equation 3.4 needs the to be rewritten as:

$$\mathrm{ODD} = \mathrm{OD}_a - \mathrm{OD}_b = \log\left(\frac{\mathrm{I"}_0\mathrm{I'}_b}{\mathrm{I"}_a\mathrm{I'}_0}\right) = \log\left(\frac{\mathrm{I'}_b}{\mathrm{I"}_a}\right) - \log\left(\frac{\mathrm{I'}_0}{\mathrm{I"}_0}\right) = \log\left(\frac{\mathrm{GL'}_b}{\mathrm{GL"}_a}\right) + \log\left(\frac{\mathrm{I"}_0}{\mathrm{I'}_0}\right) \tag{3.7}$$

where the apexes refer to the acquisitions before (') and after (") irradiation.
The second logarithmic term cannot be obtained directly empirically, but it can be evaluated with the GL of the reference strip:

$$\mathrm{ODD} = \log\left(\frac{\mathrm{GL'}_b}{\mathrm{GL"}_a}\right) + \log\left(\frac{\mathrm{GL"}_{strip}}{\mathrm{GL'}_{strip}}\right). \tag{3.8}$$

The GL values of the strip are not taken in single points; in order to have a better precision, GL values of the same column are extracted from the two images. Then the GL values of the strip imaged at time *t"* are plotted vs those of the strip imaged with *t'*, as shown in figure:

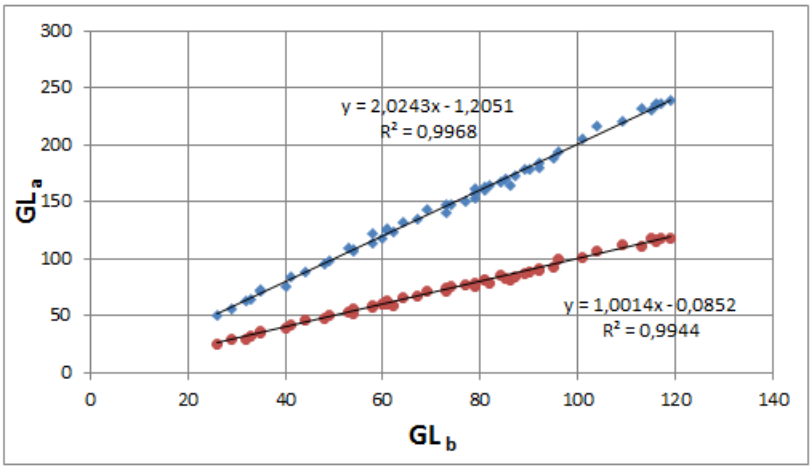

Figure 3.3: GL values of the reference strip

The red figure represents the plot of GL values of images taken with the same exposure times t', while for the blue figure the image after the irradiation was taken with exposure time $t'' > t'$. The slope of each graph represent the average value of the ratio GL''_{strip}/GL'_{strip}, so that 3.8 can be written as:

$$\text{ODD} = \log\left(\frac{GL'_b}{GL''_a}\right) + \log(slope). \tag{3.9}$$

We can easily see that, for equal exposure time, no correction with the GL values of the reference strip may be needed; for the blue graph, with different exposure times, the slopes logarithm works as correction factor. In case of equal exposure times, it is nevertheless appropriate to control, since power voltage fluctuations may have occurred; if necessary correction with the same equation 3.9 has to be made.

Cuvette GL values are extracted analytically by means of a software that extract profiles from images in a given chosen position. Due to the relatively large width of cuvettes, it is possible to pick manually GL matrix columns in a central position. Data are extracted in form of numerical vectors and are then elaborated in Excel spreadsheets. With straw dosimeters this is not possible, because of their peculiar geometry (i.e. thin cylinders). The qualitative difference in the analysis of the two different types of dosimeters is shown in figure:

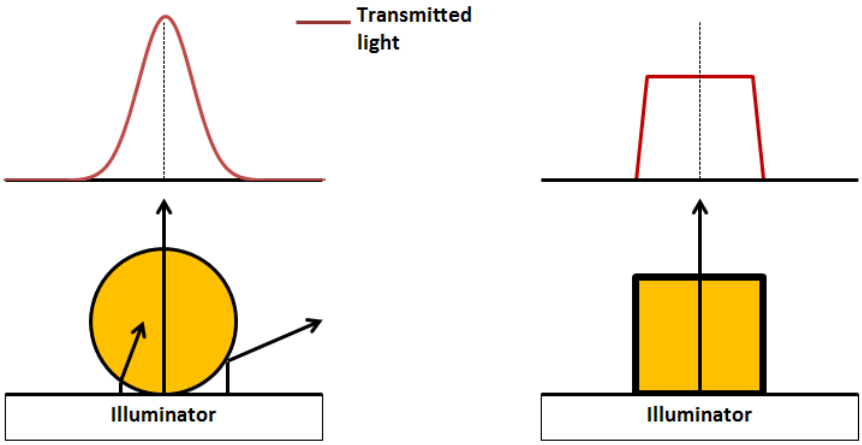

Figure 3.4: How light is transmitted through dosimeters.

Dedicated Matlab codes, reported and commented in the Appendix, have been designed to calculate ODD in straws. This type of dosimeters have circular section: these codes, given the unavoidable uncertainties of the straw positioning on the light source, are able to identify the axis of the dosimeter, calculating then the longitudinal ODD profile. Theoretically, profiles could be calculated with GL values picked from any position, but the most convenient position is the longitudinal axis, where the optical path and the absorbance are maximum, and the measure incurs in less error.
The developed Matlab code analyses each row of the dosimeter's image, and each row is a numerical vector that represents a transversal GL profile(see fig. 3.4). The code then finds the row maximum, consisting in the pixel with the maximum GL value and its 2 adjacent pixels, one each side. These three values are then saved for each row, and the resulting matrix represents the GL values profile of the dosimeter. The ODD is then calculated, pixel-to-pixel, as the logarithm of GL values and then averaged on each row, and the vector containing each row's averaged ODD represents the ODD profile on the straw axis.
The obtained ODD profiles are then reported on Excel spreadsheet for further analysis. .

3.4 Determination of the Boron dose component

When dosimeters are irradiated with a gamma source, gamma dose is found to be directly proportional to the ODD; standard and borated dosimeters will each have their own proportionality coefficient:

$$\text{Standard}: \quad D_\gamma = \alpha_{std} \bullet ODD_{std}$$
$$\text{Borated}: \quad D_\gamma = \alpha_{bor} \bullet ODD_{bor}$$

Where α_{std} and α_{bor} are the proportionality coefficients, defined as Gray per ODD unit [Gy/ODD] (see section 4.1).
In epithermal neutron fields, both dosimeters, being water equivalent, are sensitive also to the dose due to the fast neutron component, often not negligible. Borated dosimeters are sensitive also to thermal neutron radiation because of the boron reaction, and the final ODD of borated dosimeters has contributions by both gamma, fast neutron and boron dose components. The sensitivity to the boron dose is lower than the sensitivity to gamma radiation, due to the higher LET of the boron reaction products. Since both standard and borated dosimeters are equally sensitive to fast neutron dose, in the subtraction operation, aimed to obtain the boron dose, this contribution does not affect the separation result.
The ODD of the borated dosimeter can thus be expressed as function of gamma and boron doses, not considering the fast neutron dose:

$$ODD_{bor} = \frac{1}{\alpha_{bor}} (D_\gamma + \mathbf{0.41} \bullet D_n) \tag{3.10}$$

The calibration coefficient for boron dose is then lower than the coefficient for gamma dose by a 0.41 factor. Such factor was experimentally determined by previous studies [15]. For the gamma dose D_γ, for straws we utilise the measure of an adjacent standard dosimeter, for the gamma field can be considered constant; With cuvettes, having a larger width, it was necessary to utilise the gamma dose measured by a standard dosimeter in the same configuration. The obtained gamma dose can be substituted in equation 3.3 by $\alpha_{std} \bullet ODD_{std}$. Then the boron dose can easily be deducted from the previous relation:

$$D_n = \frac{ODD_{bor} \bullet \alpha_{bor} - ODD_{std} \bullet \alpha_{std}}{0.41} \tag{3.11}$$

This equation is the basis of the boron dose separation that was carried out with our experimental data. It is valid both on averaged ODD values and on ODD profiles, where separation is made point to point. Separation data has usually a larger error than gamma dose, since it is not detected directly and is a linear combination of quantities, each having its own uncertainties: boron dose graphs will thus result more scattered.

Chapter 4

Characterization of the FriXy dosimeters

In order to characterize the behaviour of the Frixy dosimeters in form of straws and cuvettes, several preliminary studies have to be carried out for both types. These include:

- Calibration.
- Linearity studies.
- Saturation trial.
- Study of the dosimeters' stability over time.

4.1 Calibration

Since sets of dosimeters from different preparations show slight variations in sensitivity, mainly due to uncertainties in weighting millimolar amounts, a different calibration is necessary for each set. Assuming dosimeters from the same set (and thus the same solution) to have the same behaviour, calibration is carried out with a small subset of the dosimeters and extended to the whole set. In our case the calibration was performed at the Fondazione IRCCS Istituto dei Tumori, in via Venezian, Milan. The FriXy dosimeters were irradiated with γ-rays from a radiotherapy unit with increasing doses; The following tables and

figures report the calibration data of subsets of straws and cuvettes from two gel preparations.

Dosimeter	Set	Dose [Gy]	ODD
9	std	23.51	0.1125
10	std	23.51	0.1136
11	std	23.51	0.1143
12	std	16.03	0.0721
13	std	16.03	0.0751
14	std	16.03	0.0750
15	std	8.55	0.0371
16	std	8.55	0.0392
49	B	23.51	0.0926
50	B	23.51	0.0888
51	B	23.51	0.0915
52	B	16.03	0.0615
53	B	16.03	0.0617
54	B	16.03	0.0627
55	B	8.55	0.0375
56	B	8.55	0.0307

Table 4.1: Calibration of standard and borated straw dosimeters

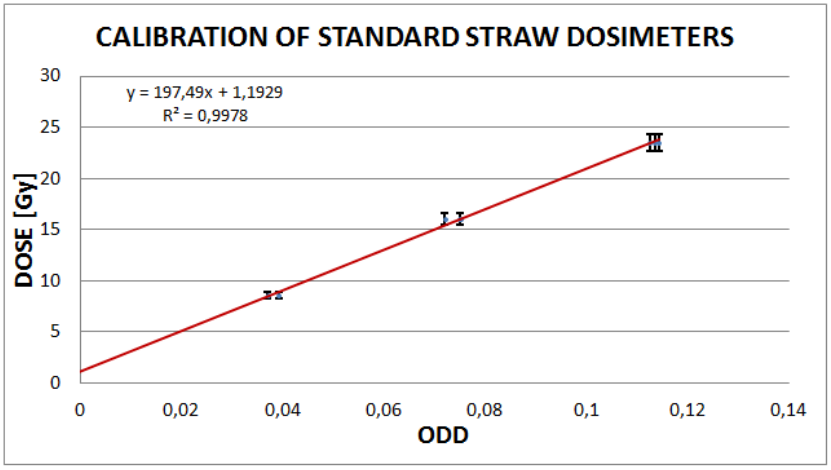

Figure 4.1: Calibration of standard straw dosimeters

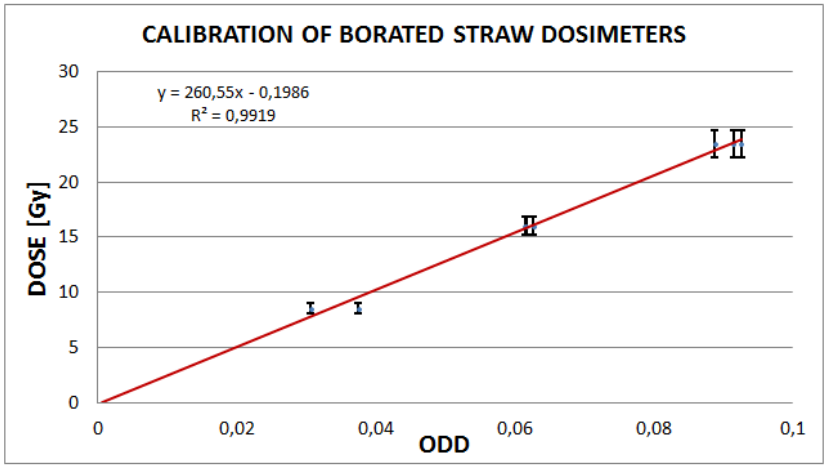

Figure 4.2: Calibration of borated straw dosimeters

The average sensitivity of the standard straw dosimeters is 214.96 Gy/ODD with a standard deviation of 7.86 Gy/ODD, and a relative uncertainty of 3.6% ; The borated dosimeters show an average sensitivity of 258.62 Gy/ODD, standard deviation of 13.21 Gy/ODD and a relative uncertainty of 5.1%.

Calibration of standard and borated cuvette dosimeters

Dosimeter	Set	Dose [Gy]	ODD
5	std	11.75	1.1712
6	std	11.75	1.1671
7	std	5.34	0.5478
8	std	5.34	0.5674
25	B	11.75	0.8299
26	B	11.75	0.8659
27	B	5.34	0.4228
28	B	5.34	0.4736

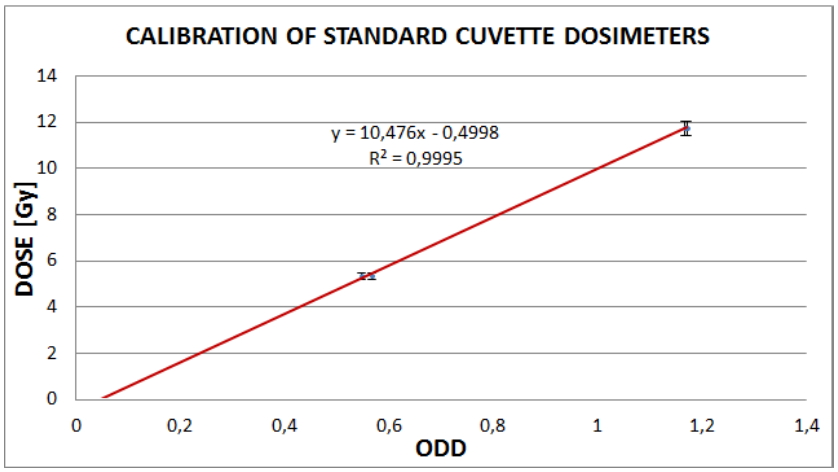

Figure 4.3: Calibration of standard cuvette dosimeters

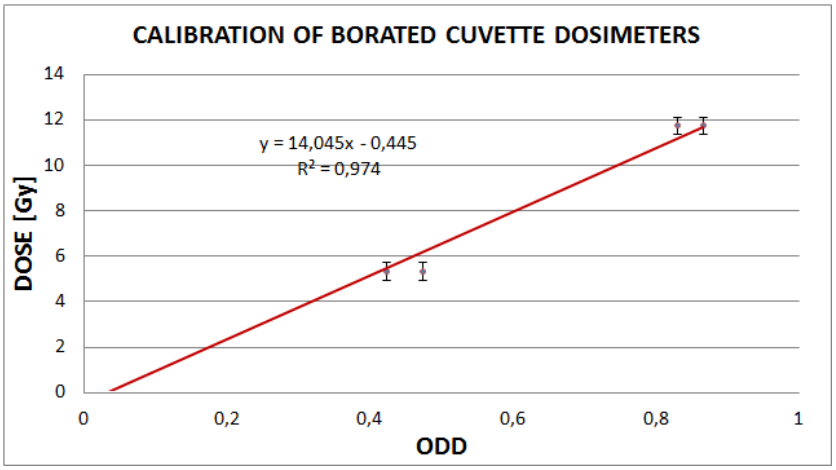

Figure 4.4: Calibration of borated cuvette dosimeters

The average sensitivity of the standard cuvette dosimeters has resulted to be 10.476 Gy/ODD (Gray per ODD unit) with a standard deviation of 0.264 Gy/ODD, with a relative uncertainty of 2.6% . The borated dosimeters show the beginning of saturation behaviour; the trend-line intercept has been imposed to zero, and the data at higher doses have an higher dose to ODD ratio; this leads to a larger dispersion of data from the calibration value adopted, and thus to larger uncertainty. The adopted value of sensitivity is 14.045 Gy/ODD, standard deviation of 1.203 Gy/ODD and a relative uncertainty of 11%.

These calibration data (along with another analogous data set) have been used to calculate doses at the research center in Řež.

4.1.1 Correction of sensitivity non-uniformities

After the calibration, performed with uniform irradiation with gamma rays, ODD profiles along the dosimeters were imaged in order to check the uniformity in sensitivity. Straw dosimeters sensitivity was found to have good spatial uniformity; cuvette dosimeters were found to have a sloped ODD profile, and therefore to have a non-uniform sensitivity along the axis. This distortion was found equally in standard and borated dosimeters. To correct this distortion, a correction string for each kind of dosimeter was obtained. This string is a function of the position along the dosimeter, and it is reported in the following figures for standard and borated dosimeters.

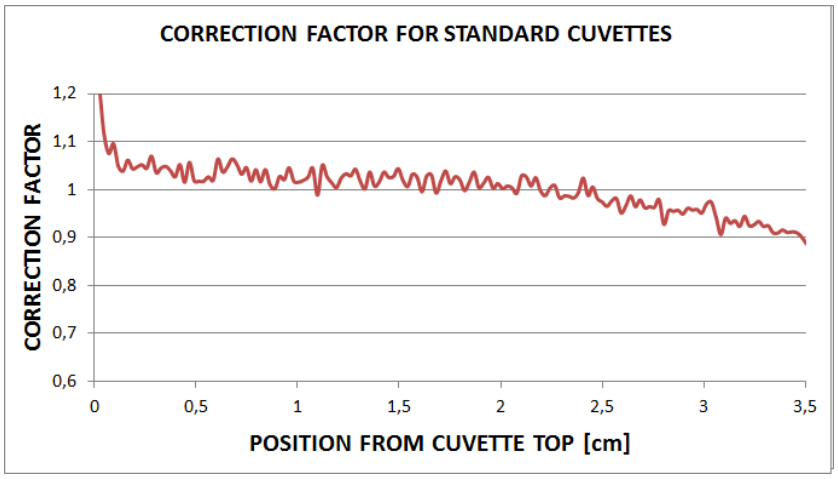

Figure 4.5: Correction string for standard cuvette dosimeters

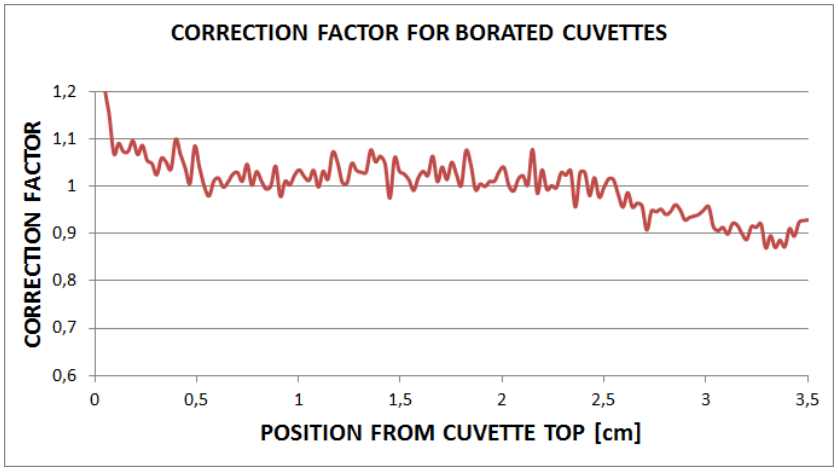

Figure 4.6: Correction string for borated cuvette dosimeters

The correction string is normalised to the average value.
The dose rate distributions reported in chapter 5 were obtained multiplying the measured ODD distributions, along the cuvettes, by these correction strings.

4.2 Linearity and Saturation doses

In order to extensively study the dosimeters' behaviour, preliminary studies of linearity were carried out in the months prior to the Řež irradiations. While linearity of Fricke gel dosimeters had already been verified in other dosimeters shape, straw dosimeters required characterization, given the differences in dimensions and geometry with cuvettes and other previously used dosimeters. These studies were also used to optimize the image acquisition device (CCD camera + computer) configuration, to maximise resolution for small dosimeters; the analysis process was also developed in this phase, with the creation and continuous improving and simplification of Matlab codes.
Also cuvettes needed characterization, mainly with the aim of finding the linearity ODD range (and correspondent dose range), predictably shorter than straws' range, because of the longer optical path, and then higher light absorbance. It is possible to observe that cuvette dosimeters are subject to saturation problems at lower doses due to their width, and their saturation is an optical saturation rather than a chemical one, since dose range for a Fricke

dosimeter is estimated to be up to 400 Gy.

4.2.1 Linearity and saturation for cuvette dosimeters

A numerous set of dosimeters was irradiated by a Caesium-137 (^{137}Cs source at Fondazione IRCCS Istituto dei Tumori in Milan with increasing doses. The irradiation was performed in cylindrical geometry, and the uniformity of dose distribution within each dosimeter, and among dosimeters was ensured. The absorbed dose was proportional to the irradiation time, with a dose rate of ~ 0.126 Gy/s. Results are shown in the following figures. It is possible to observe that cuvette dosimeters are subject to saturation problems at lower due to their width, and their saturation is an optical saturation rather than a chemical one, since dose range for a Fricke dosimeter is estimated to be up to 400 Gy.

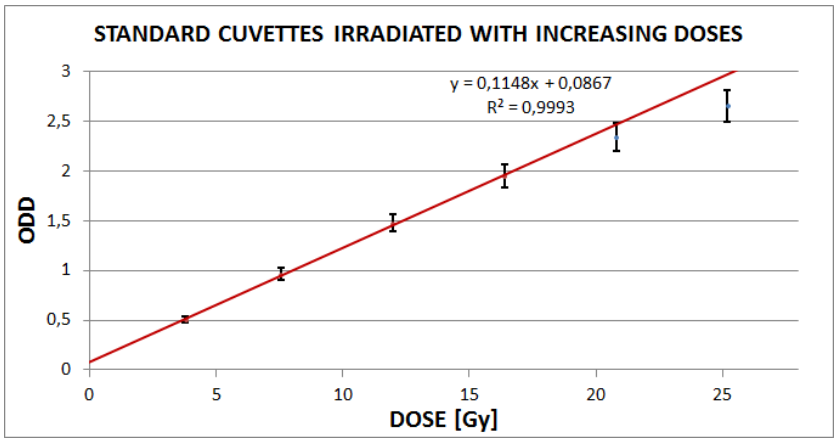

Figure 4.7: ODD of standard cuvette dosimeters irradiated with increasing doses

Every point in the figures is an average value of the ODD of those dosimeters irradiated for the same time; from this figures is immediately evident a saturation behaviour, for standard cuvettes, starting from certain values of ODD, around 2.
The corresponding irradiation time of 180 seconds corresponds to a dose of about 22.68 Gy.

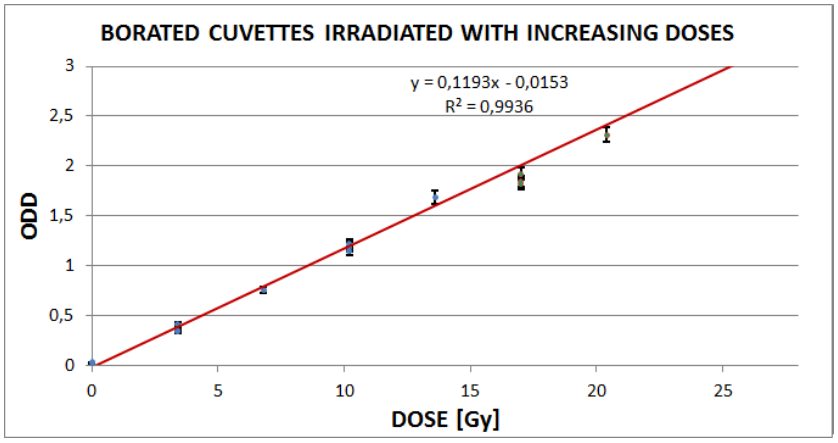

Figure 4.8: ODD of borated cuvette dosimeters irradiated with increasing doses

Borated cuvettes show good linearity up to ODD values of around 2, corresponding to a dose of ~15.12 Gy; extending the linearity to dose values up to induces little error.

4.2.2 Linearity and saturation of straw dosimeters

Straw dosimeters are less affected by optical saturation because of their limited thickness, but it is still possible to identify a certain ODD range where they show a linear behaviour. Owing to the fact that, for straw dosimeters, low doses correspond to very low ODD values (~ 0.01), straw dosimeters are less reliable at low ODD values, i.e. low doses. This is also reflected in the relative errors found, often high at low doses, then decreasing in the linearity range. Errors are large at high doses, out of the linearity range. Results for standard straw dosimeters are shown in figure 4.7. Standard straw dosimeters show linear trend in the ODD range 0.02-0.0879, corresponding to a dose range between ~ 7.57 Gy and ~ 31.5 Gy.

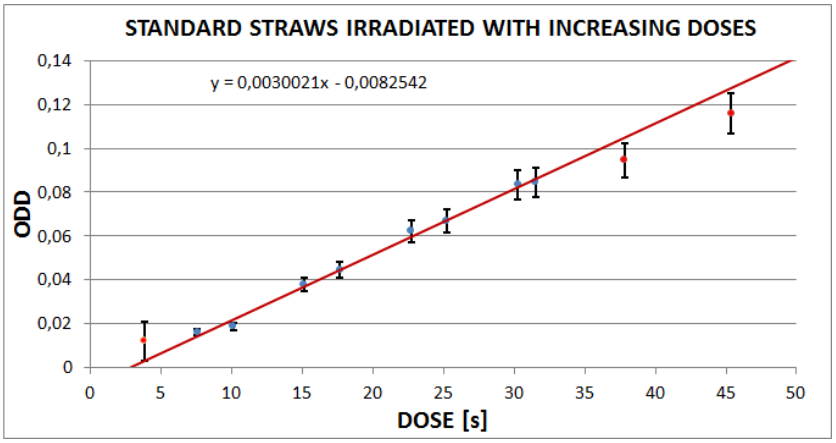

Figure 4.9: ODD of standard straw dosimeters irradiated with increasing doses

Results for borated straw dosimeters are shown in figure 4.8.

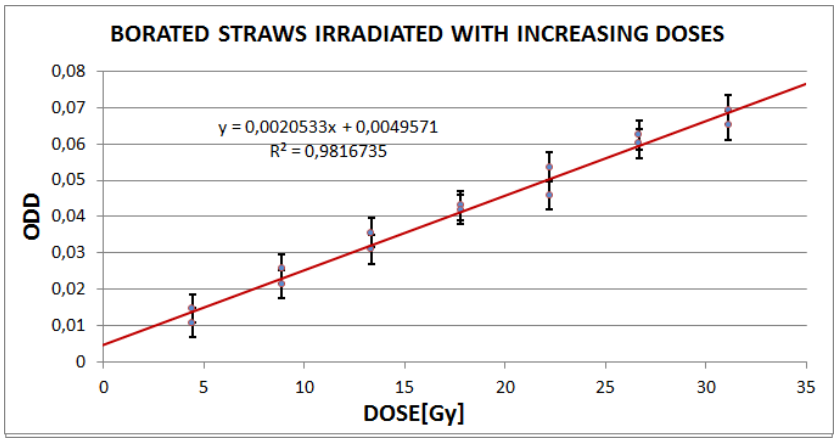

Figure 4.10: ODD of borated straw dosimeters irradiated with increasind doses

Borated straw dosimeters show good linearity up to 0.07 in ODD value, corresponding to a dose of ~ 30 Gy. The linearity range is then the same of the standard straws.

From the calibration and linearity studies, it can be seen that the sensitivity of standard dosimeters, expressed in ODD/Gy, is higher than the sensitivity of borated dosimeters. This means that, being the ODD linearity range almost equal between standard and borated dosimeters, the dose range of the borated dosimeters is larger.

4.3 Stability over time

Since the purpose of this thesis was to perform measurements at a nuclear reactor facility where it wasn't possible to calibrate dosimeters with a gamma source of known dose rate, so calibration had to be performed at the laboratory in Milan, a few days before or after the experiments. It was then necessary to study how gel dosimeters characteristics evolves in time, performing calibration on several days after the gel preparation, to assess variations in sensitivity. Ageing of the gel matrix affects the dosimeter sensitivity with several effects:

- decreased precision: dosimeters irradiated with equal doses will show an increasing spread of ODD values, mainly do to oxygen penetrations because of sealing imperfections, and to oxygen permeability of the container walls.
- decreased range: ageing works as an additional dose increasing with time, lowering the effective dose range. This effect is mainly due to auto-oxidation of the dosimeter.
- sensitivity nonuniformities: dosimeters must be kept in a cool place (e.g. refrigerator) with a high degree of temperature uniformity. Poor cooling quality may result in local sensitivity irregularities in the single dosimeter.

A previous study on Fricke gel dosimeters, carried out in the laboratory, showed that sensitivity has an initial growth during the during the first day after the preparation, the it maintains stable and starts slightly decreasing on days 3/4 after the preparation. To investigate the variation in sensitivity in time, a set of dosimeters was subjected to irradiation in different days, a subset being irradiated the day after preparation, the other subsets 4, 5 and 6 days after. The irradiation days were chosen to reproduce the same conditions to which the dosimeters irradiated in Řež were subjected, being irradiated 4 or 5 days far from the calibration.
The dosimeters for this study were kept in optimal cooling conditions. This optimal conditions were not available for the dosimeters that were utilised in Řež, that spent the whole journey in a cooling bag carefully arranged to ensure to

the best possible thermal conditions, and then in Řež the cooling conditions were slightly worse, because of the small space available in the refrigerator. We assumed nonetheless that the results of this study could be profitably utilised to infer the calibration value to be utilised for the measurements in Řež.

4.3.1 Stability over time for straw dosimeters

The following figures report the data from the irradiation of standard and borated straw dosimeters.

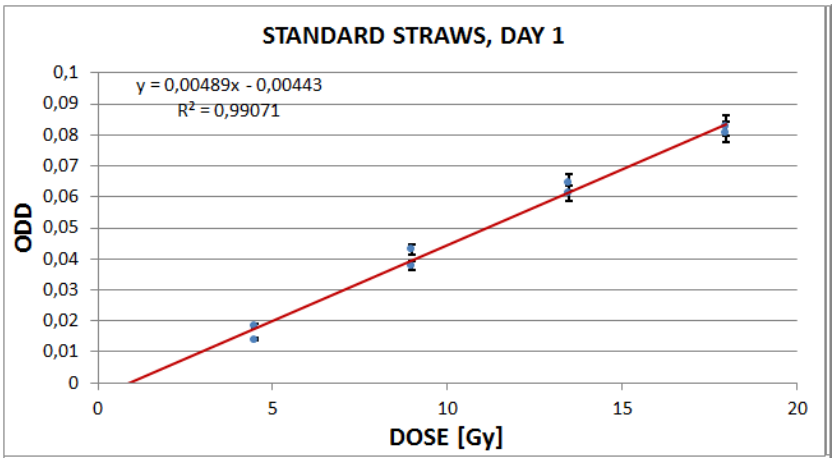

Figure 4.11: ODD of standard straw dosimeters irradiated 1 day after preparation

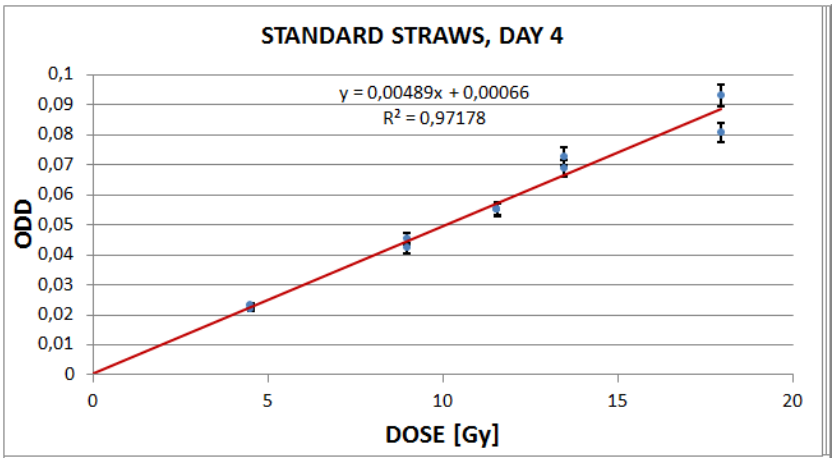

Figure 4.12: ODD of standard straw dosimeters irradiated 4 days after preparation

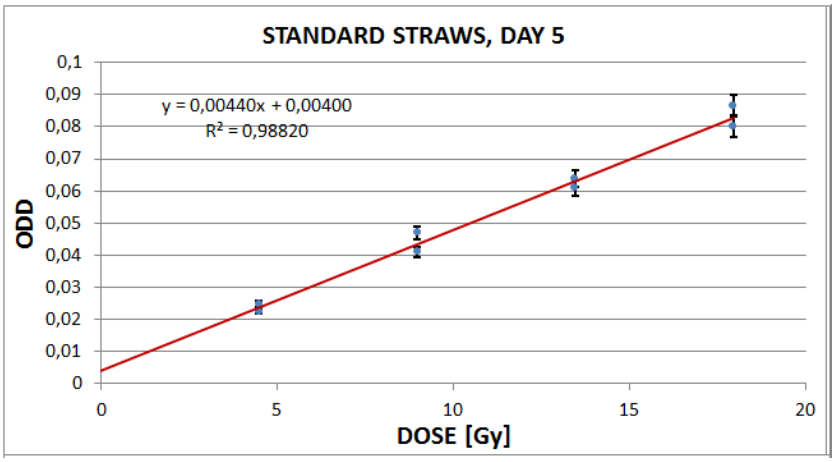

Figure 4.13: ODD of standard straw dosimeters irradiated 5 days after preparation

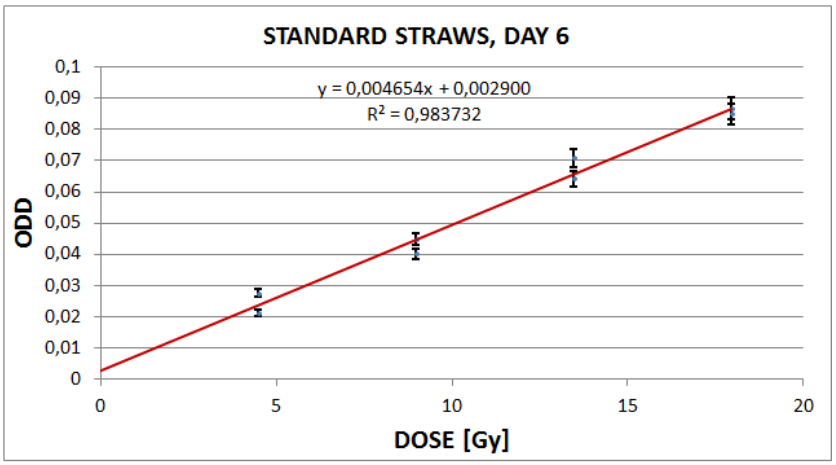

Figure 4.14: ODD of standard straw dosimeters irradiated 6 days after preparation

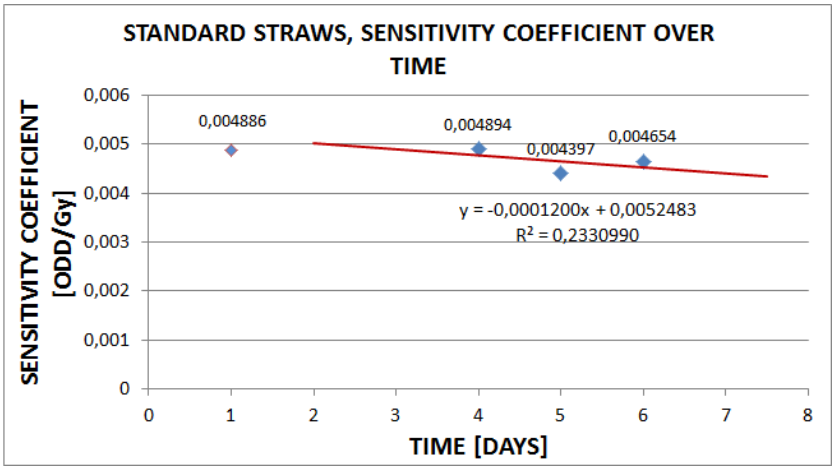

Figure 4.15: Standard straw dosimeters sensitivity coefficient over time, calculated as unit of ODD per Gray

The trend line is fitted on data from days 4,5 and 6. It is possible to observe that the sensitivity on day 4 is constant respect of day 1, then there is a slight decrease in value. Respect of the sensitivity measured on day 1, the relative variation of sensitivity on day 5 is ~10%, on day 6 is ~5%. For the correction of the calibrated sensitivity, for measures performed a few days after the preparation, the angular coefficient of the trend line is used as correction factor. This means for standard dosimeters, a correction of the sensitivity of about -2.5%

per day after day 4.

Data for borated straws are reported in the following figures:

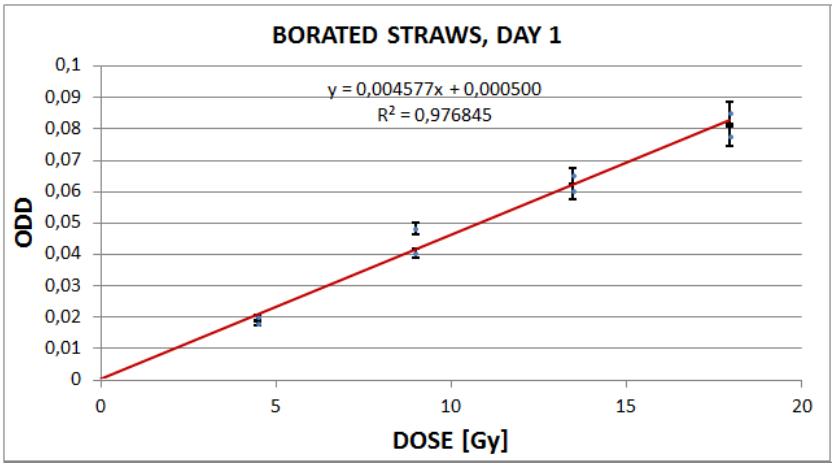

Figure 4.16: ODD of borated straw dosimeters irradiated 1 day after preparation

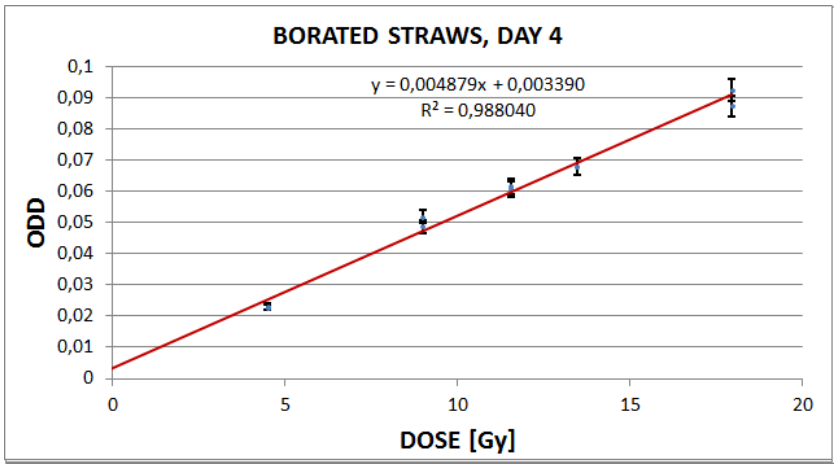

Figure 4.17: ODD of borated straw dosimeters irradiated 4 days after preparation

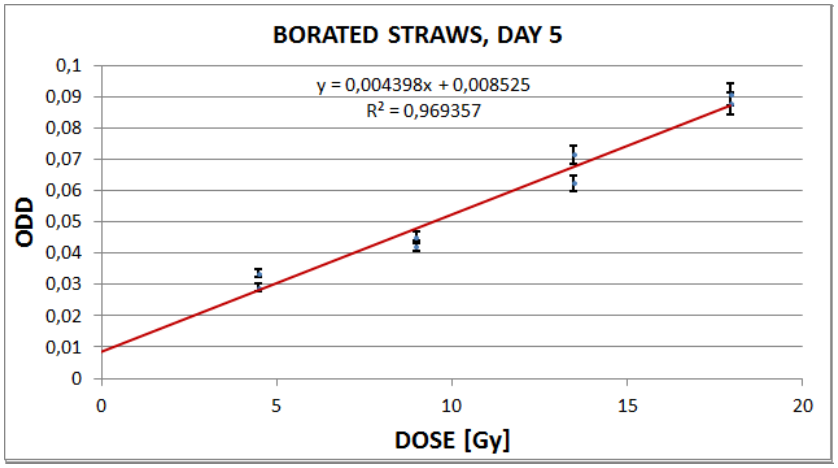

Figure 4.18: ODD of borated straw dosimeters irradiated 5 days after preparation

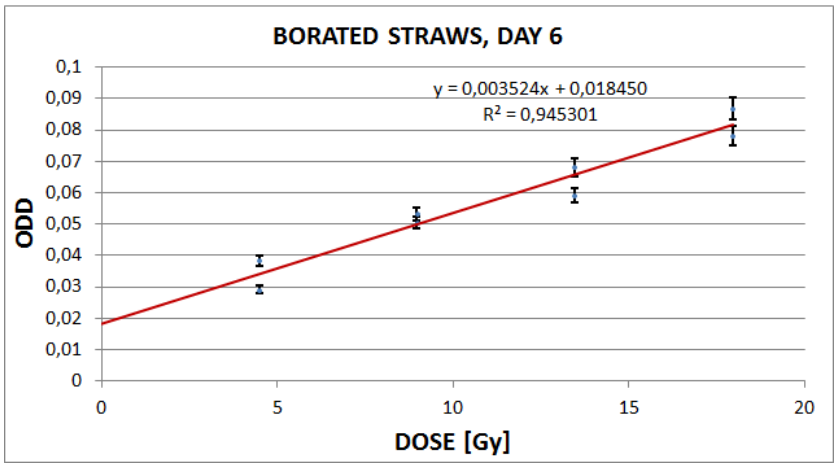

Figure 4.19: ODD of borated straw dosimeters irradiated 6 days after preparation

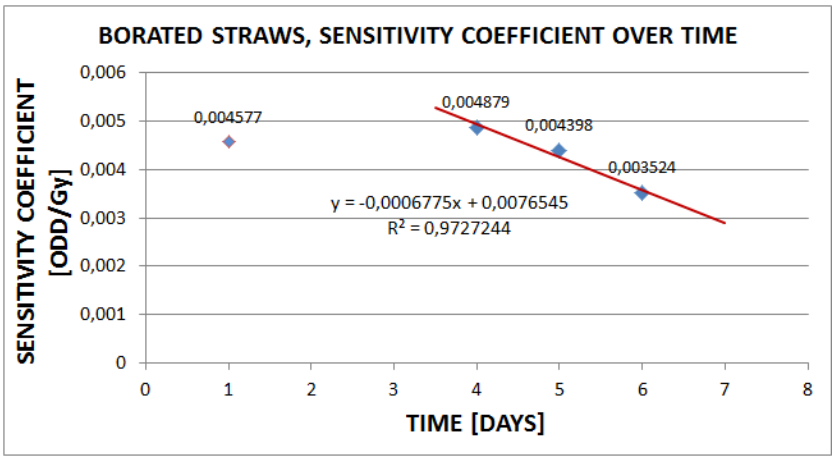

Figure 4.20: Borated straw dosimeters sensitivity coefficient over time, calculated as unit of ODD per Gray

For borated dosimeters the variation of sensitivity, compared to the sensitivity measured on day 1, is ~4% on day 5, and ~23%. The correction of the sensitivity for borated dosimeters is of about -14% per day after day 4.

4.3.2 Stability over time for cuvette dosimeters

Cuvette dosimeters are less affected by deterioration: cuvettes are designed for scientific applications, in which the specimens purity is to be kept. Straws are produced for industrial application, and the straw plastic could be permeable to oxygen.
The following figures report the data from the irradiation of standard and borated cuvette dosimeters.

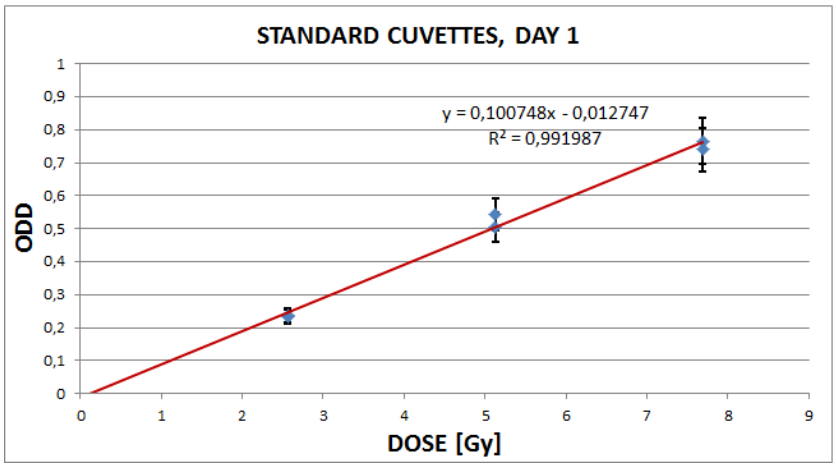

Figure 4.21: ODD of standard cuvette dosimeters irradiated 1 day after preparation

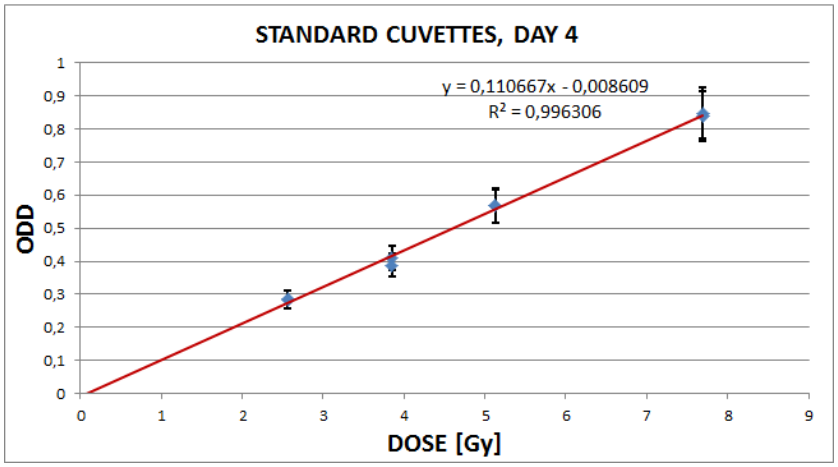

Figure 4.22: ODD of standard cuvette dosimeters irradiated 4 days after preparation

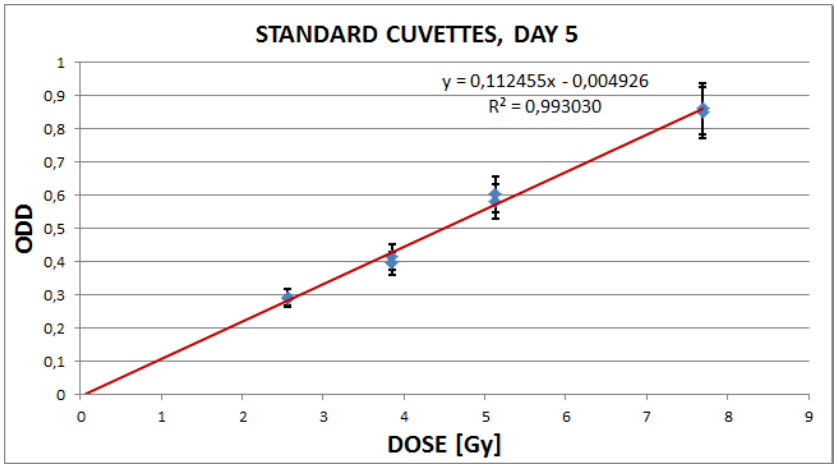

Figure 4.23: ODD of standard cuvette dosimeters irradiated 5 days after preparation

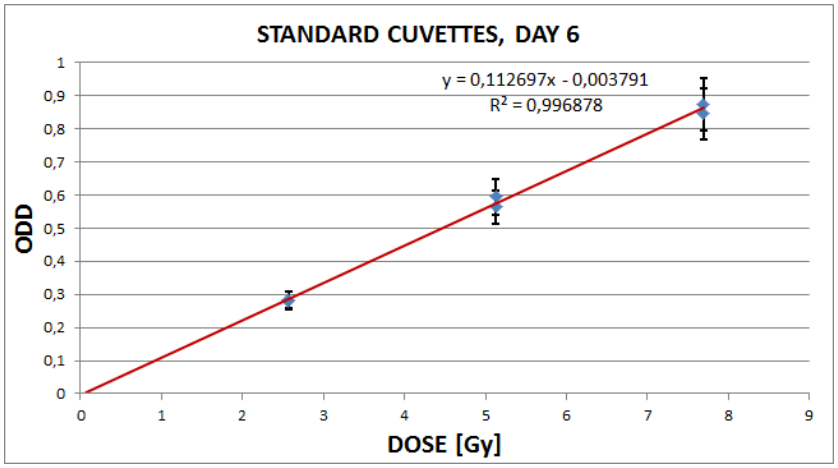

Figure 4.24: ODD of standard cuvette dosimeters irradiated 6 days after preparation

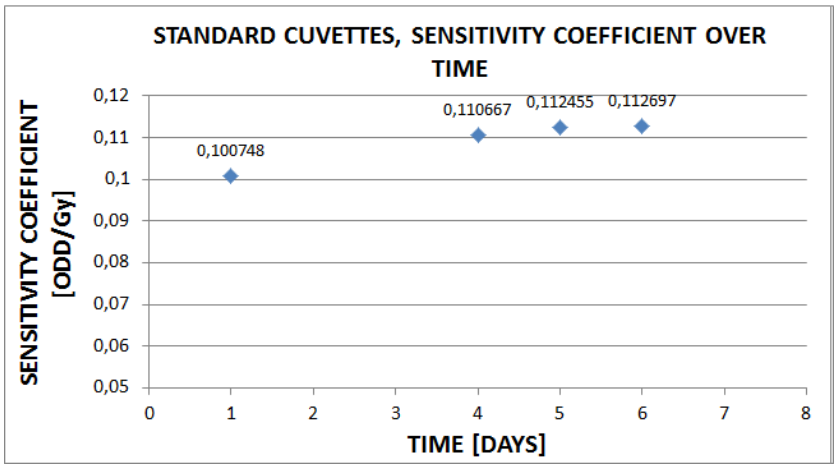

Figure 4.25: Standard cuvette dosimeters sensitivity coefficient over time, calculated as unit of ODD per Gray

Standard cuvette dosimeters show a slight increase in sensitivity from day 1 to days 4, 5, 6. Sensitivity during days 4, 5, 6 is considered constant, because variations are into the error margin. The increase in sensitivity from day 1 to days 4, 5, 6 is ~10%.
Data for borated cuvettes are reported in the following figures:

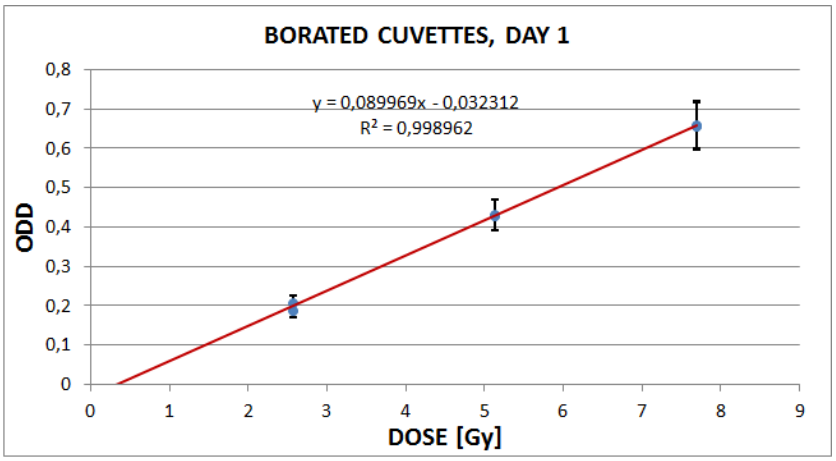

Figure 4.26: ODD of borated cuvette dosimeters irradiated 1 day after preparation

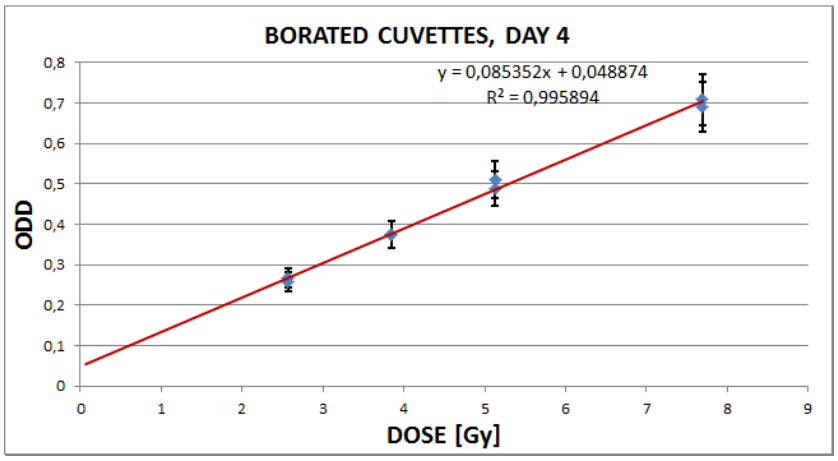

Figure 4.27: ODD of borated cuvette dosimeters irradiated 4 days after preparation

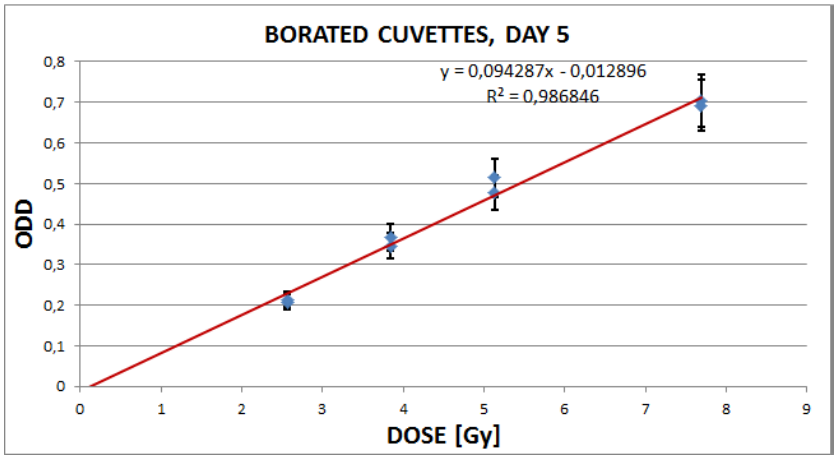

Figure 4.28: ODD of borated cuvette dosimeters irradiated 5 days after preparation

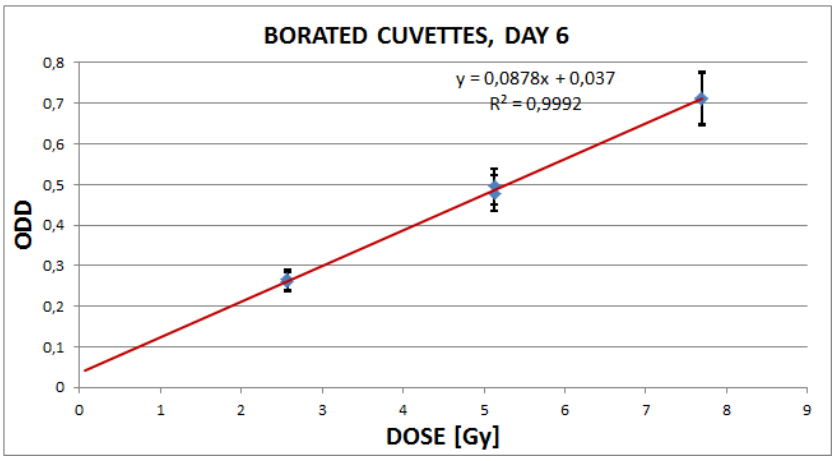

Figure 4.29: ODD of borated cuvette dosimeters irradiated 6 days after preparation

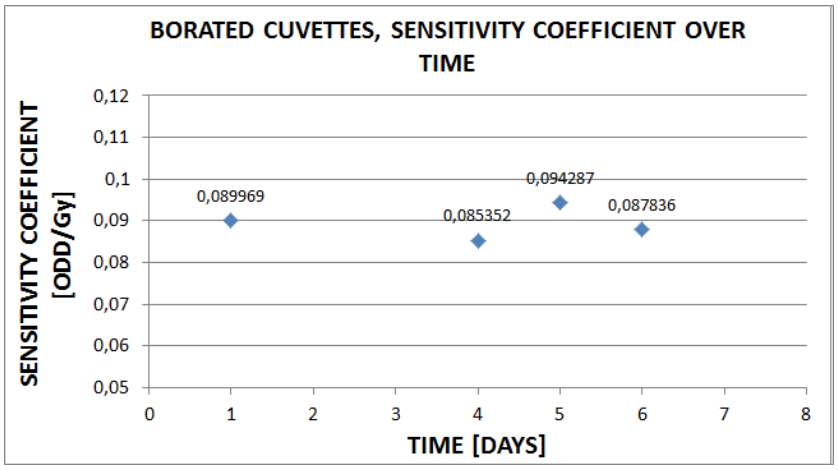

Figure 4.30: Borated cuvette dosimeters sensitivity coefficient over time, calculated as unit of ODD per Gray

Borated cuvette dosimeters sensitivity seems constant over time. Relative variations of sensitivity in days 4, 5, 6, respect to day 1, are ~5%, within the error margin. Therefore, no correction of sensitivity is needed for calibration data.

Chapter 5

Experimental Campaign in Řež

During a week in June 2012, irradiation experiments were carried out in Řež Nuclear Research Center. In order to challenge the effectiveness of a new boron carrier for BNCT, Prof. Mares (Institute of Physiology, Academy of Science, Prague) and collaborators at LVR-15 designed irradiation trials in different configurations on living targets such as cell cultures or little mice to study the biological response. Cell cultures were arranged in two types of containers, while mice were irradiated with or without partial shielding of the body. In 2011, similar experiments were arranged and little Cadmium cylinders were chosen as shielding agents; Cadmium showed himself not to be a suitable shield for living things, since it proved to be very effective in stopping neutrons, but its gamma emissions, due to neutron activation, caused very high dose. In 2012 Cadmium cylinders were replaced by hard paper cylinders covered with a granular Borated layer, certainly less effective in thermal neutron shielding but without undesired gamma emissions. Figures 5.1, 5.2 show the biological system on which Prof. Mares studies were focused.

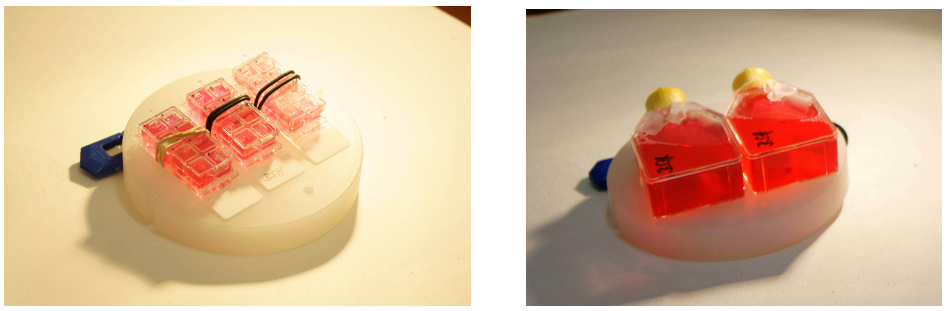

(a) (b)

Figure 5.1: Pictures of cell specimens to be irradiated in multi-cell boxes (a) and in flasks (b)

Figure 5.2: Picture of mice in borated paper cylinders, with the polyethylene irradiation container in the back

Figure 5.3: How the irradiation container was positioned towards the beam

The goal of this experimental campaign was to evaluate the absorbed dose in samples for biological experiments, as said before, the samples were little mice and cell cultures in small containers. To this aim we designed and prepared gel phantoms in which the absorbed dose can be measured with the suitably designed dosimeters, previously described. To achieve this goal we had to replicate as faithfully as possible each irradiation geometry (see section 1.3.3) of the biological experiments, using the same containers, or very similar ones, and substituting biological tissue (e.g. mice or cell culture) with tissue equivalent gel (made with Gelatine from Porcine Skin).
The irradiation experiments carried out in Řež are reported and analysed in the following sections. They can be summarized as:

- Cuvettes and straws in mouse-shaped gel phantoms
- Cuvettes and straws in mouse-shaped gel phantoms with borated shield
- Straws in flasks for cell cultures
- Straws in cuvettes simulating multi-cell boxes for cell cultures

It is important to point out that irradiation times were decided on the basis of results obtained from the irradiations performed one year before. Approximate doses were deduced from these data in order to decide the duration of the first irradiation in order to remain in the dosimeters' linearity range without incurring in saturation. On the basis of the results of the first irradiation, the durations of all the following exposures were established. We have taken into consideration that the Reactor operation power had been raised from 9 to 10 MW, leading to an increase of neutron flux and gamma background somewhat proportional to power variation, but not known for certain.
Cuvettes were irradiated for 1 hour, while straws for 2 hours; to account for neutron flux fluctuations due to reactor power instabilities, dose rates were normalised to an effective irradiation time, determined comparing the count rate of a monitoring detector during the irradiation to its nominal value at nominal power:

$$T_{eff} = \frac{C_{tot}}{c_{nom}} \tag{5.1}$$

Where C_{tot} is the total number of counts in the irradiation time and c_{nom} is the nominal count rate.

5.1 Moderation of the epithermal neutron beam of the LVR-15 reactor

As said in section 1.2, in BNCT treatments of deep tumor, epithermal neutron beams are preferred to thermal beams because of the necessity to penetrate tissues a few centimetres in depth. The irradiation samples of our experiments were only 1-2 cm thick, and therefore the epithermal neutron beam required thermalisation . For biological experiments, it was then necessary to provide a moderating medium before the beam mouth, and the irradiation box was then designed with a 2 cm thick polyethylene bottom and 13 cm radius.

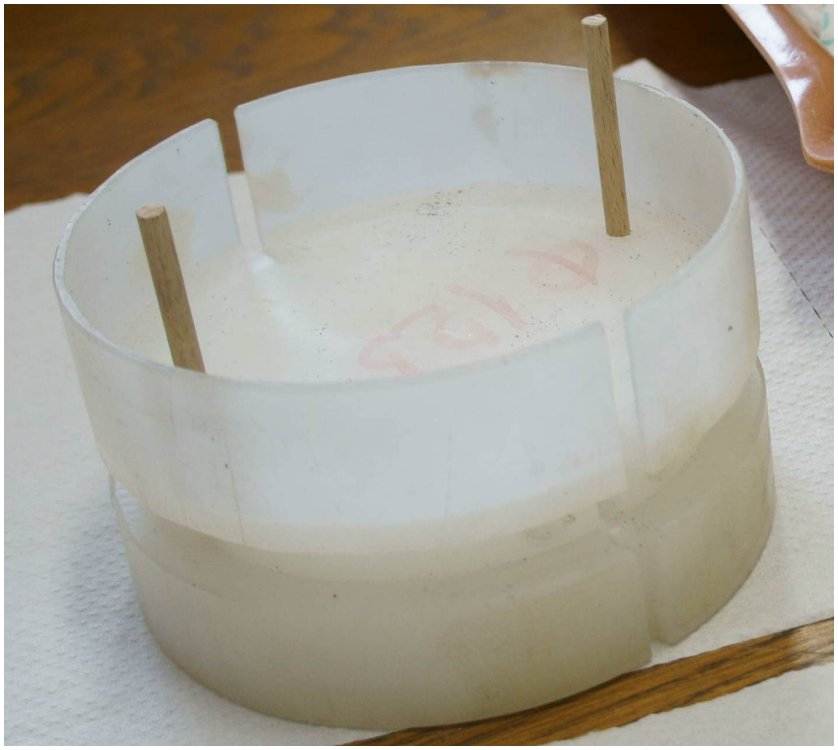

Figure 5.4: Picture of the irradiation box

Measures with thermoluminescence dosimeters were performed to obtain dose distribution profiles of the beam, in an other study.

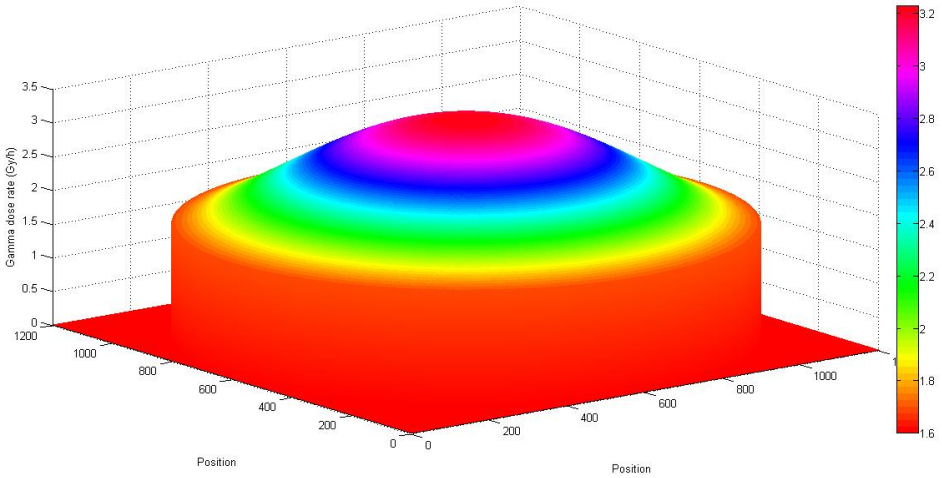

Figure 5.5: Gamma dose rate of the moderated beam

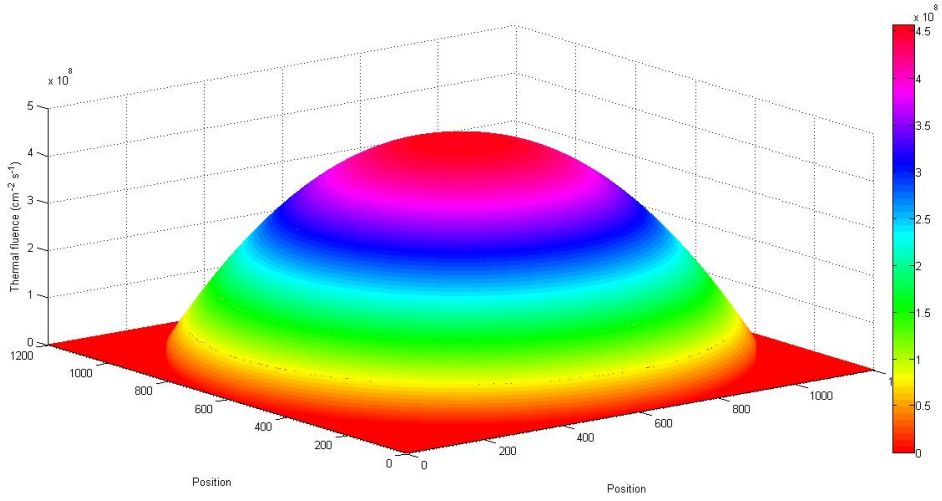

Figure 5.6: Thermal fluence per second of the moderated beam

The gamma dose distribution has a continuous trend peaked in the center. The Gamma dose rate at the peak is ~3.2 Gy/h, while it is ~1.7 Gy/h in the peripheral zone. The ratio between the centred value and the peripheral value is ~1.9 . Also the thermal neutron dose distribution has a peaked shape: the peak value is ~4.5•10^8 neutrons per cm^2 per second, the peripheral vale is ~1•10^8 neutrons per cm^2 per second. The ratio between centred and peripheral values is ~4.5 . Since boron dose rate distributions are strictly related to the thermal neutron flux, it is important to consider such gamma and thermal neutron distributions for the interpretation of the results obtained, specially those obtained in mice phantoms (section 5.4 and 5.5).

5.2 Fast neutron contribution evaluation

In past studies, methods for fast neutron separation have been studied by means of gel dosimeters made with heavy water instead of water [**?**]. This dose component is not sensibly affected by the size of the phantom or by the irradiation geometry, since fast neutrons aren't affected much by backscattering. Data from previous studies (Bartesaghi et al, 2009 [17]) can be used to estimate the fast neutron dose for our irradiations.

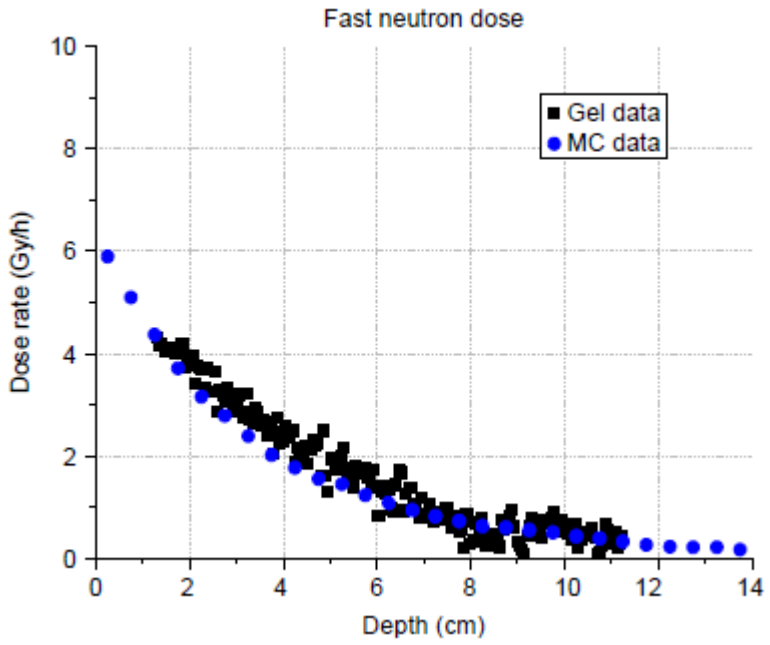

Figure 5.7: On-axis fast neutron distribution taken in cylindrical phantom. The relative fast neutron dose was measured with Fricke gel dosimeters and calculated by means of Monte Carlo simulations; results are shown normalised at 1.25 cm of depth.

This figure reports fast neutron dose distribution with depth in water phantom, measured with the same neutron beam in Řež. Gel dosimeters are less sensitive to fast neutron dose than to gamma dose by a 0.85 factor; we can summarize the total measured dose by standard and borated dosimeter as:

$$D_{std} = D_{\gamma} + 0.85 \bullet D_{fast} \tag{5.2}$$

$$D_{bor} = D_{\gamma} + 0.41 \bullet D_{n} + 0.85 \bullet D_{fast} \tag{5.3}$$

Boron dose D_n calculation, as defined in equation 3.4, is not affected by fast neutron dose, since both standard and borated dosimeters are sensitive to it. To determine gamma dose D_γ however, fast neutron dose must be subtracted from the total dose measured by standard dosimeters. To determine from the figure fast neutron dose absorbed by a dosimeter in an experimental config-

uration, the total thickness of water equivalent materials, between the beam collimator mouth and the dosimeter, has to be considered. Dosimeters were inserted inside gel phantoms, of variable thickness, placed in the polyethylene container of cylindrical geometry, with a thickness of 2 cm. The following table reports the different phantoms shapes that were used in the irradiation, each corresponding to a total depth of water equivalent material (2 cm of polyethylene + gel phantom thickness between the dosimeter and the moderator), leading to a corresponding fast neutron dose, extracted from figure 5.7.

	Total Depth (cm)	**D_{fast} (Gy/h)**	**Correction on D_{std} (Gy/h)**
Flasks	2	~3.3	-2.805
Mice phantoms	3.3 (average)	~2.8	-2.38
Cuvettes	2	~3.3	-2.805

where the correction on D_{std} is the fast neutron dose corrected by the 0.85 factor. The depth for mice phantoms is the average radius.

5.3 Straws in flasks for cell cultures

In the original setup cell cultures were deposited on one side of the flasks forming a thin layer (~ μm), the flask was filled with a water solution and part of the flask was screened with the borated paper shield. To replicate this geometry, flasks were filled with gel and straw dosimeters were put in the gel on one side of the flask, against the wall. The aim of the experiment was to determine boron and gamma dose distributions along dosimeters length, partly shielded and partly in the non-shielded region.
Experimental setups are shown in the following pictures:

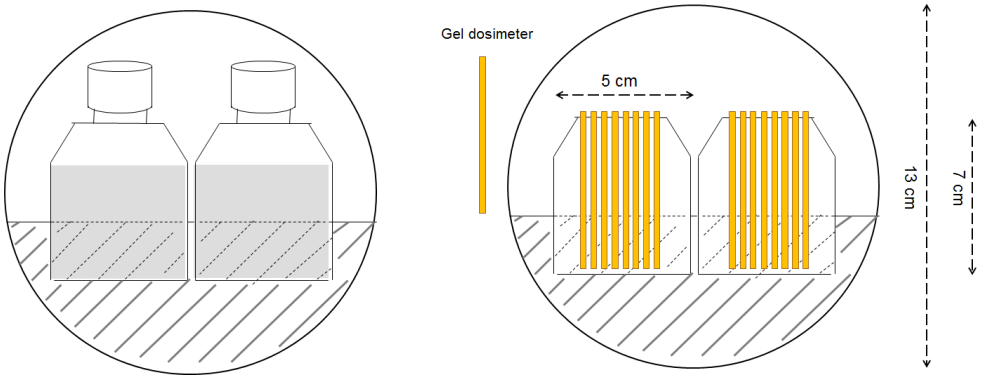

(a) (b)

Figure 5.8: Scheme of the original irradiation setup (a) and of our reproduction (b)

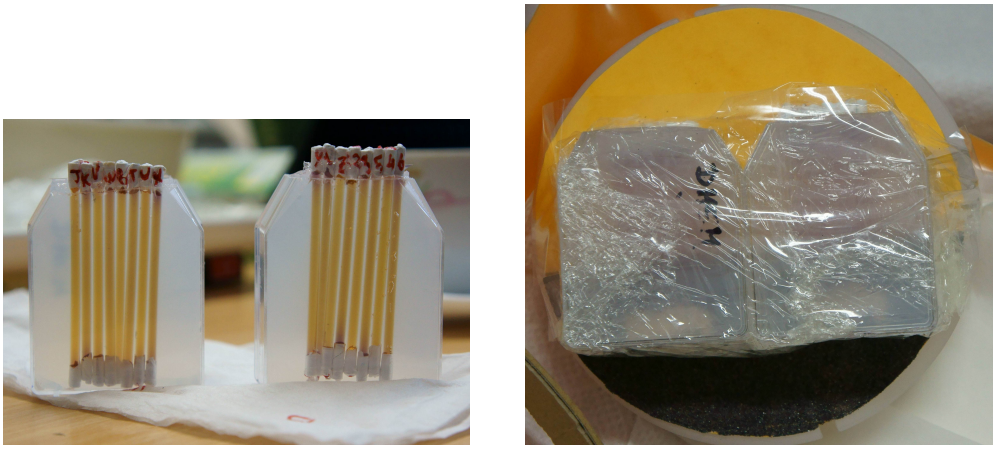

(a) (b)

Figure 5.9: Picture of straw dosimeters in the flasks (a) and of the flasks ready for irradiation (b)

Sixteen dosimeters, half standard and half borated, in this configuration were irradiated for 2 hours. Two of them showed broad irregularities and were therefore discarded. The following figure reports dose rate results averaged of the remaining dosimeters.

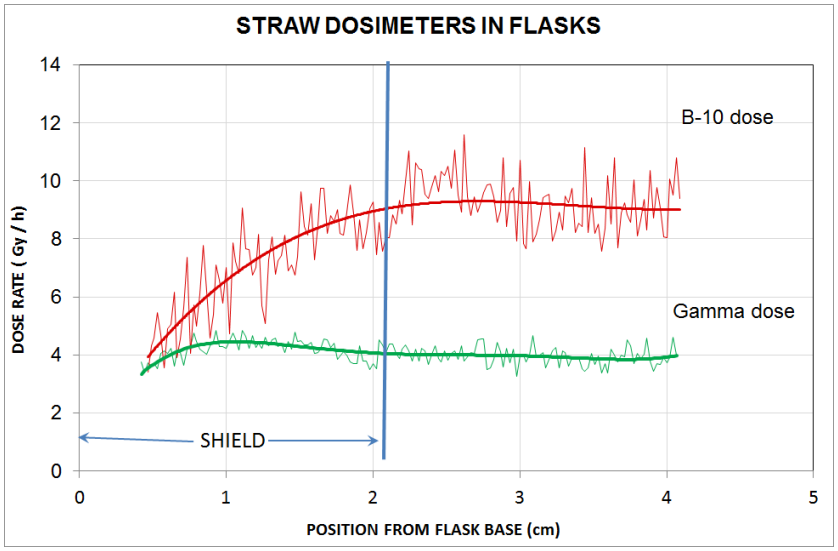

Figure 5.10: Dose rate profiles from straw dosimeters in flasks

The gamma dose rate was measured by standard dosimeters, and the boron dose was deducted from dose separation between adjacent dosimeters. Dose values were then averaged on couples of dosimeters. Low variability in dose values between dosimeters were found. Relative uncertainties are ~7.5% for standard dosimeters and ~13.6% for borated dosimeters.
It is possible to observe from the figure that the two dose components are almost constant outside the shielding, while the boron dose drops in the shield region, proving some shielding effectiveness by the borated paper. The dose gradient in the shielded region is not steep: this is probably caused by the gel thickness (~ 2 cm), that may favour neutron scattering and therefore diffusion, explaining why the boron dose drops with finite slope and not abruptly towards the bottom. We can also observe a slight increase in gamma dose in the shielded region: we assumed that glue might have been used to stick the borated layer onto the support paper, and mostly glues may incur in activation if irradiated with thermal neutrons.

5.4 Cuvettes and straws in mouse-shaped phantoms

In the original setup 4 little mice were irradiated in the irradiation container separated by a frame of cardboard. To replicate the irradiation geometry, we made mice-shaped gel phantoms in which straw or cuvette dosimeters were positioned, with the aim of determining the dose rate distributions of gamma radiation and boron dose, over the whole body.
Experimental setups are shown in the following pictures.

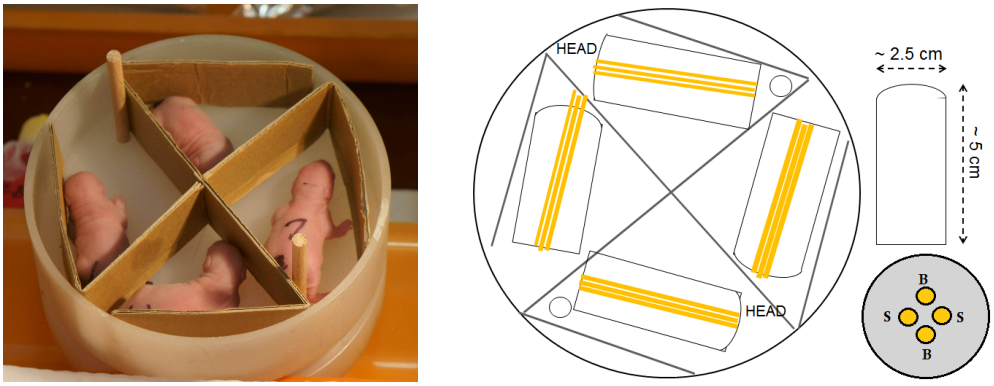

(a) (b)

Figure 5.11: Picture of naked mice in the irradiation setup (a) and scheme of the reproduced setup with straw dosimeters in mice-phantoms (b). On the right, the positioning of straw dosimeters in each phantoms is reported, were S are the standard dosimeters and B are the borated dosimeters.

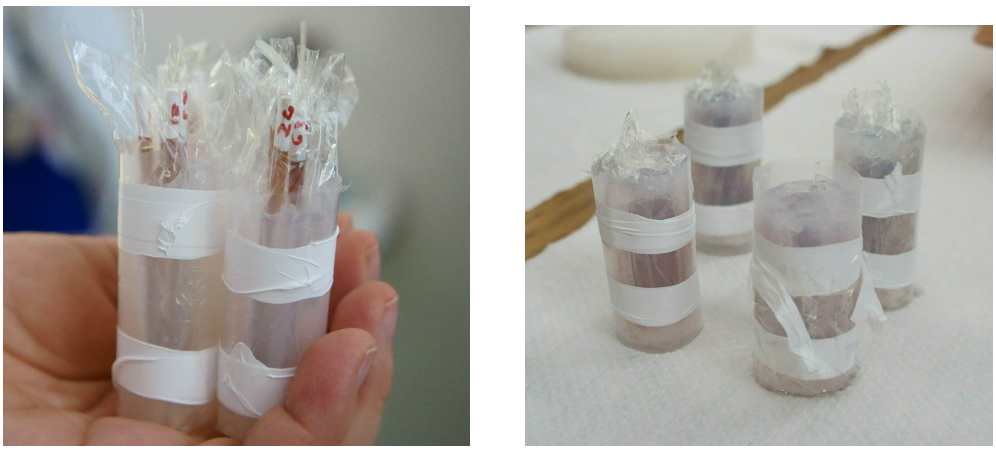

(a) (b)

Figure 5.12: Pictures of mice phantoms with straw (a) and cuvette dosimeters (b)

Four mice phantoms with cuvettes were irradiated for 1 hour in this configurations, two of them standard and two borated. Mice phantoms were arranged in couples, putting their heads adjacent, improving symmetry for a more reliable subsequent dose separation. The dose rate distribution is reported in the following figure.

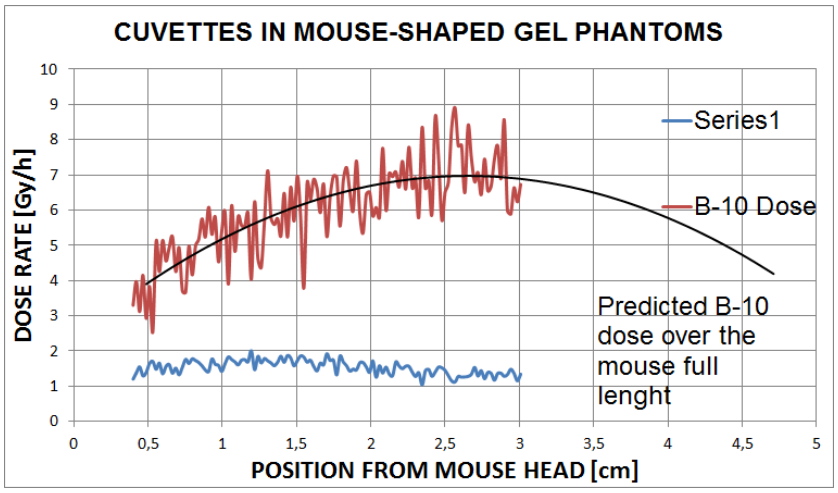

Figure 5.13: Dose rate profiles from cuvettes in mice phantoms

Cuvettes are shorter than mice phantoms, and the black line represent the dose rate extrapolated profile over the mouse full length, because the irradia-

tion configuration is symmetric respect to mice phantom center;. Gamma dose is shown to be spatially constant, while neutron dose profile is has a maximum at the center. This is reasonable if we consider the thermal neutron fluence distribution reported in section 5.1.
We may use the dose rate we found to calculate the neutron thermal flux using the *kerma factor*, with the relation described by Matzumoto et al., 1985 [16]:

$$D = 1.602 \bullet 10^{-10} E\ F\ N\sigma\Phi = k_f\Phi \tag{5.4}$$

$$k_f = 1.602 \bullet 10^{-10} E\ F\ N\sigma \tag{5.5}$$

where D is the absorbed dose [Gy], E is the average kinetic energy transfer of charged particles [MeV], F is the weight fraction of a considered isotope, N is its number of atoms per gram, σ is the cross section of a considered reaction [cm^2], Φ is the neutron fluence [cm^{-2}] and k_f is the kerma factor [Gy/cm^2]. Kerma (acronym of *Kinetic Energy Released in MAtter* can be defined as the sum of the initial kinetic energies of all the charged particles liberated by uncharged ionizing radiation, such as neutrons or photons. Kerma and Dose are roughly equivalent in our case, while kerma can be much higher for high energy gamma rays, as some of the energy escapes the considered volume as fast electrons or bremsstrahlung X rays. Kerma factor k_f is defined as kerma per unitary fluence; in our dosimeters, with 40 ppm of ^{10}B, we have $k_f = 3.45 \bullet 10^{-12}$ Gy/cm^2, where this value of k_f is obtained utilising as value for E a reviewed valued of 2.34 MeV. Considering the maximum obtained dose rate as D' ~7 Gy/h, we obtain the neutron fluence:

$$\Phi = 2 \bullet 10^{12} \text{ neutrons per } cm^2 \text{ in 1 hour}$$

which means a corresponding flux:

$$\phi = 7.3 \bullet 10^{15} \text{ neutrons per cm per second}$$

This dose rate and flux results are consistent with previous literature about LVR-15 epithermal column, as reported in Bartesaghi et al, 2009 [17], with the following figure:

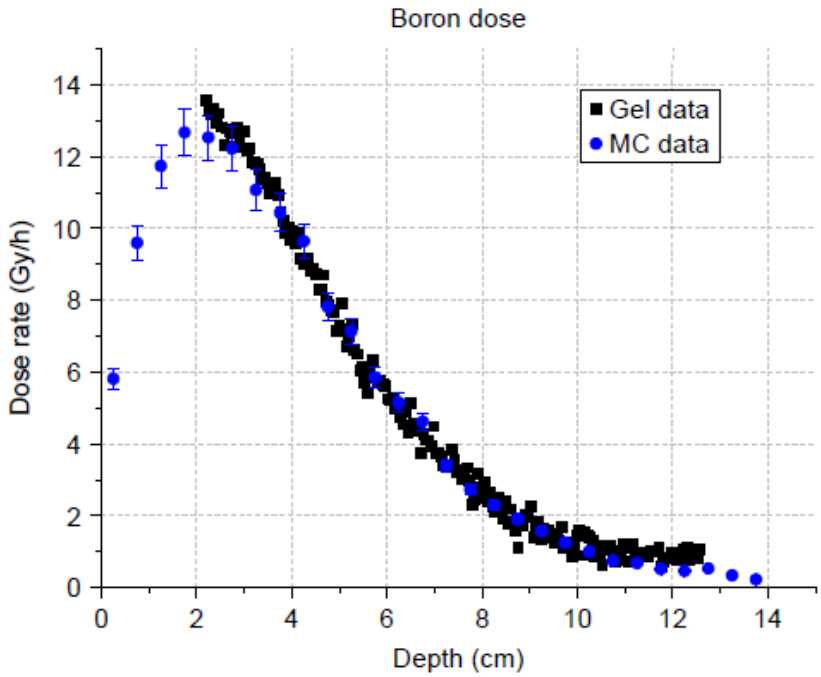

Figure 5.14: On-axis boron dose distribution measured in water phantom.

Where dose is measured at different depths in a water phantom with dosimeters with 35 ppm of ^{10}B, and the blue data are calculated with Monte Carlo simulations. The first two centimetres correspond to the plastic wall of the phantom container. The hypothetical position of our mice phantoms in this figure would be about 3.3 cm, considering the thickness of the container wall (2 cm), and the phantom radius (~1.3 cm): dose rate reported in this position are higher than our measurement, even at lower boron concentration. This is plausible, considering the different geometry of the irradiation, i.e. 50×50×25 cm^3 water phantom: in such geometry, thermal neutron flux is higher because of backscattering , thus boron dose is sensibly increased. Data from our measurements are of the same order of magnitude, hence we can assume them to be consistent with these data, considering the different irradiation geometry.

Sixteen straws were irradiated for 2 hours in this geometry (see fig. 5.11), four in each mouse, equally divided between standard and borated. The irradiation time was of 2 hours. The reported figures are from averaged data from a subset

of these dosimeters:

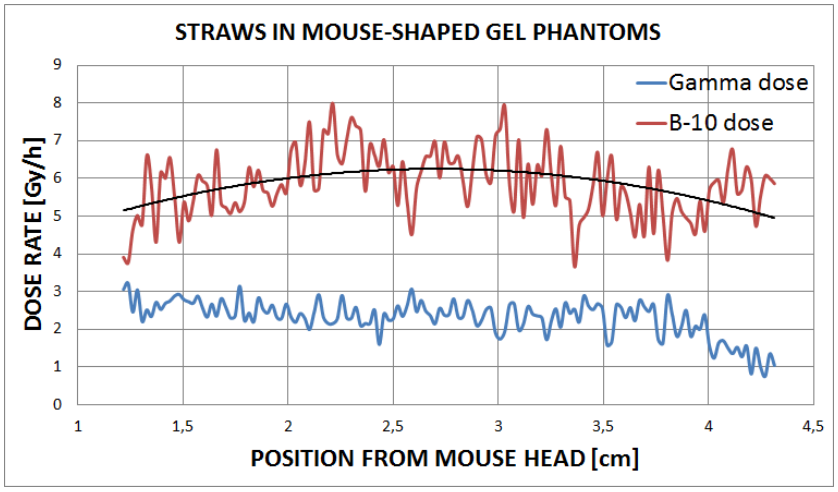

Figure 5.15: Dose rate profiles from straws in naked mice phantoms

Where the uncertainty on data is ~10%. Neutron dose seems to be coinciding within the error with cuvette data, while gamma dose is slightly higher. This is probably caused by activation of the straw plastic, as a matter of fact straws showed an activity higher than cuvettes when checked with a portable detector after irradiations.

5.5 Cuvettes and straws in mouse-shaped gel phantoms with borated shield

In the original setup 4 little mice were irradiated with the same configuration of that described in section 5.4; in this case mice were placed into shielding cylindrical open-top boxes, made with the borated paper, of 2.8 cm diameter and 4 cm of height. The mice heads were left outside the shielding box, as irradiation target. To replicate the irradiation geometry, mice gel phantoms were placed into the shielding boxes, and the dosimeters were placed into the phantoms. To simulate the position of the mice heads, outside the box, dosimeters were placed with one end exceeding the box about ~1.5 cm. The irradiation setup is exemplified by the photo and schemes below.

Figure 5.16: Photo of cuvette dosimeters in mice phantoms, with shielding

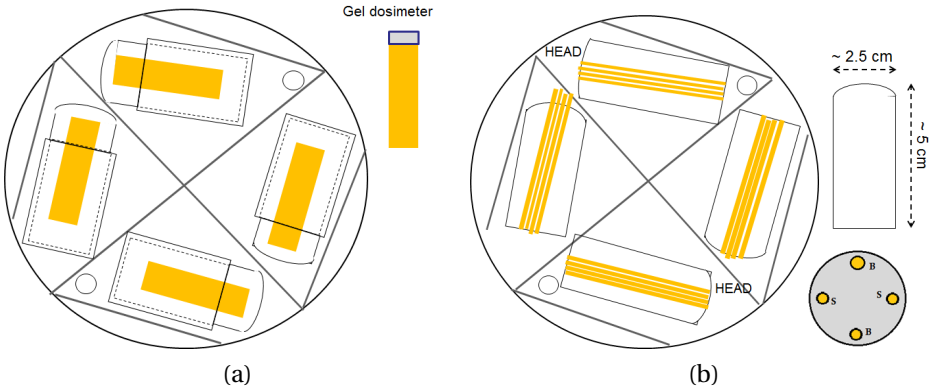

(a) (b)

Figure 5.17: Scheme of the reproduced setup, in mice-phantoms with shielding, with cuvette (a) and straw dosimeters (b). On the right, the positioning of straw dosimeters in each phantoms is reported, were S are the standard dosimeters and B are the borated dosimeters.

With respect to what observed in section 5.1, it is possible to notice that the mice irradiation positioning is not optimized.
Four phantoms with cuvettes were irradiated for 1 hour in this geometry. As shown in figure 5.16, cuvettes were arranged in two couples, each composed by a standard and a borated dosimeter, with adjacent heads. Boron dose separation was performed between cuvettes of the same couple. The following figure

reports the dose rate of gamma and boron radiation. The position of the shielding is indicated by the blue line.

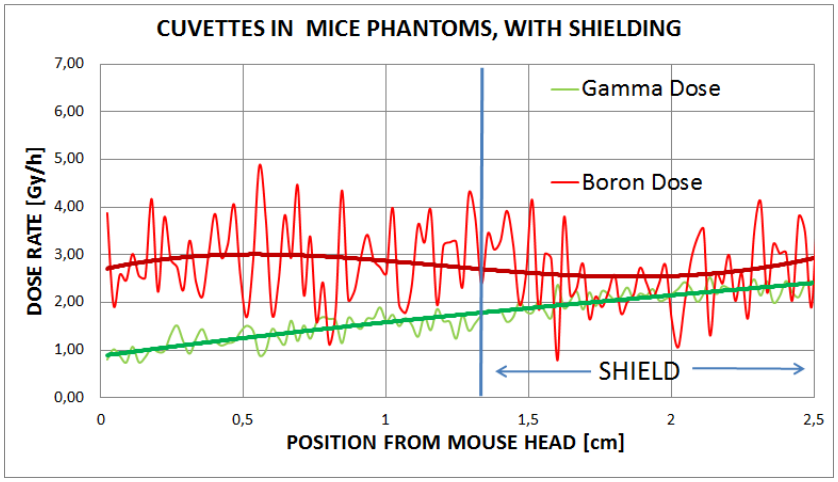

Figure 5.18: Dose rate profiles from cuvettes in mice phantoms with shielding.

The boron dose is lower in the shielded part, proving the effect of the shielding. The magnitude of the shielding effect is of ~0.5 Gy/h at most.
Gamma dose shows an increase towards the shielded region: this could be caused by activation of the shielding material component, such as glue as explained before.
Sixteen straws were irradiated for 2 hours in this geometry, four in each phantom, as described in figure 5.17. Dose data were averaged between the 2 dosimeters of the same type in each phantom, and separation was performed between standard and borated straws within each dosimeter. The following figure reports the dose rate of gamma and boron radiation. The position of the shielding is indicated by the blue line.

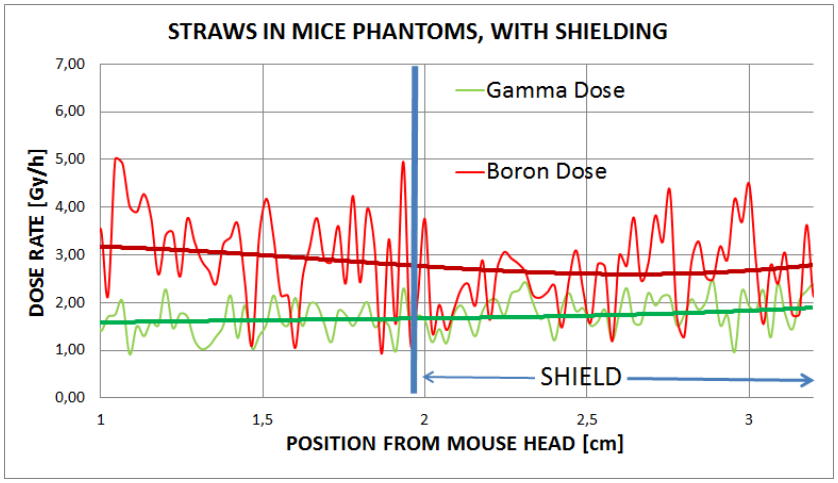

Figure 5.19: Dose rate profiles from straws in mice phantoms with shielding

As observed for cuvettes, for straws boron dose is higher in the non-shielded region. Dose rate values coincide with those measured with cuvettes.
Gamma dose shows an increase towards the shielded region also for straw dosimeters. Its value in the non-shielded region is slightly higher than measured with cuvettes, and this may be caused by activation of straws plastic.

5.6 Straws in cuvettes simulating multi-cell boxes for cell cultures for cell cultures

In the original setup cell cultures were deposited as a thin layer in the little cells of multi-cell boxes, as shown in figure 5.1(a). Since it was not possible to introduce the dosimeters in such multi-cell containers, we had to replicate the irradiation geometry with cuvettes, that are almost equal in volume, as shown in figure.

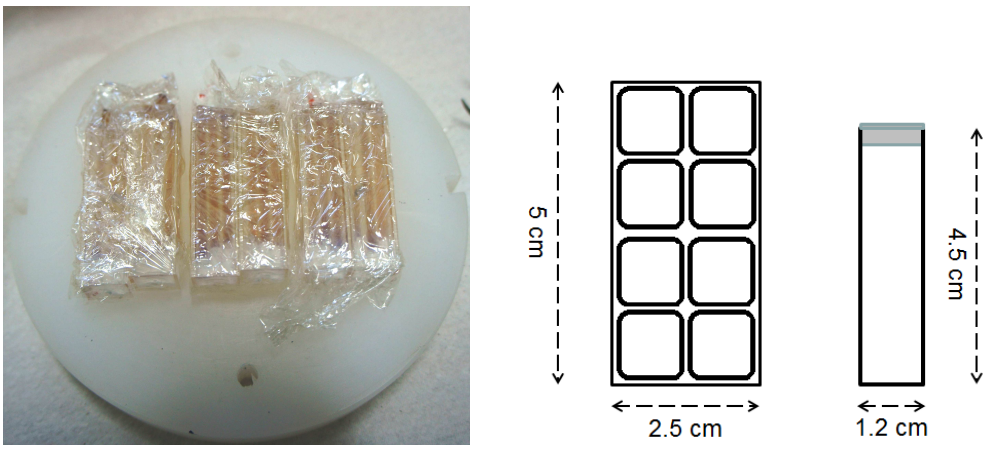

(a) (b)

Figure 5.20: Picture of straw dosimeters in cuvettes (a) and schematic comparison between multi-cell boxes and cuvettes(b)

Each multi-cell box was replicated by a pair of adjacent cuvettes. Not considering the interspaces, the two kinds of containers are almost equal in dimensions. Gel thickness seems to be slightly larger in cuvettes, about 1 mm. Eighteen dosimeters were irradiated for 2 hours, 9 standard and 9 borated, without Boron shielding. Each cuvette was filled with gel with 3 straws on one side, always alternating standard with borated dosimeters. Separation of boron dose was operated between couples of adjacent straws. Dose rate distributions for gamma and boron dose are reported in the following figure.

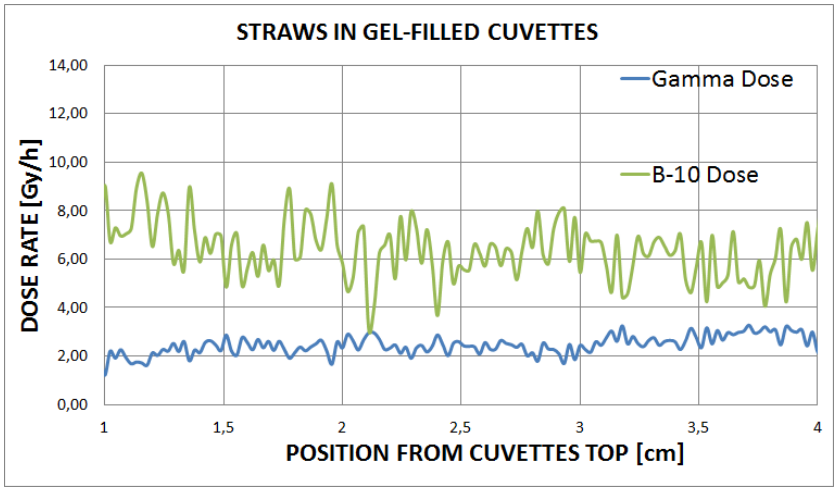

Figure 5.21: Dose rate profiles from straws in gel-filled cuvettes

Dose data at the straws extremities are discarded, due to distortion. Gamma dose is constant over the straws length, at values very similar to those observed in mice phantoms (section 5.4). Boron dose value seems constant over the dosimeters length. This is reasonable, considering that this dosimeters were positioned at the central region of the beam, where the differences in thermal flux are little compared to the peripheral zone of the beam.

Conclusions

This work focused on the development of neutron and gamma dosimetry methods, based on Fricke gel dosimeters, to study dose distributions in small targets exposed to epithermal neutron beams from nuclear reactor. Little cuvettes and straws were chosen as suitable containers. Preliminary studies were carried out with photon beams in Milan in order to characterize the dosimeters behaviour, and irradiations with epithermal neutrons were performed at the Nuclear Research Center in Řež, using the reactor's epithermal beam designed for Boron Neutron Capture Therapy (BNCT).
Gel dosimeters were optically analysed, and the linearity between ODD and absorbed dose was verified over a certain dose range. Standard and borated dosimeters showed saturation at similar ODD levels. Being borated dosimeters sensitivity inferior, the dose range of borated dosimeters is larger.
Fricke gel straw and cuvette dosimeters sensitivity trend over time was studied, to evaluate the evolution of the dosimeters sensitivity obtained with calibration, for the measures carried out in Řež, where it is not possible to perform calibrations. Cuvette sensitivity shows to remain constant, while straw sensitivity drops after a 4/5 days. Straws are more sensitive to ageing, because of a quicker oxygen contamination through the container plastic, and the sealings.
In the experimental campaign in Řež, dose profiles in small phantoms were successfully measured. The phantoms used replicated biological samples irradiated for BNCT studies. Gamma rays and Boron dose components were separated using dosimeters with different isotopic composition, while fast neutron dose component was evaluated. Dose measures were carried out in small mice phantoms and cell cultures containers, with and without shielding, and the effectiveness of the shielding was estimated. The shielding was made by means

of hard paper with a layer of boron powder. The shielding effect of this material is observable from the measurements. An effect of activation of the glue used for the shielding paper was observed.
Measures of the gamma and boron dose distributions after the moderating polyethylene layer at the epithermal column mouth will also help to better design future experiments, optimizing the irradiation geometry (see section 5.1). For example, the geometry used for mice exposures was not good: mice heads, that are the irradiation targets, have to be placed near to the beam axis, to maximize boron dose.
The results shown in this thesis demonstrate the capability of the developed method of Fricke gel dosimeters of small dimensions, in particular straw dosimeters, to measure continuous distributions of different dose components in small water equivalent phantoms, exposed to BNCT beams. These results are consistent with other measurements performed with thermoluminescence detectors. The accuracy of straw dosimeter measurements could be improved with a more accurate optical analysis, with a better camera resolution.

Appendix A

Matlab codes

This first simple software was designed to obtain ODD average values over single straw dosimeters uniformly irradiated, e.g. during calibration.

```
function[ODD]=ddocorti(name,x1,x2,y1,y2)

% name = ['a','b','c'] ; string that brings informations about which
dosimeters to analyse.
% x1, x2 = matrix columns between which the dosimeter is located
% y1,y2 = matrix rows between which the dosimeter is located
count=size(name);
sample=conta(2);    % these two lines determine the sample numerosity
alt= y2-y1+1;          % determines the dosimeters effective height
for nn=1:sample       % repeats the analysis for each dosimeter

    location = strcat ('C:\Users\raff\Desktop\tesi\dos 5 luglio\cannucce
                                \s',name(nn),'\1p.bmp');
                                % location of the photo taken before irradiation
    location2 = strcat ('C:\Users\raff\Desktop\tesi\dos 5 luglio\cannucce
                                \s',name(nn),'\1d.bmp');
                                % location of the photo taken after irradiation


    a = imread (location);  % transforms photos in numeric matrices
a(1:alt,:) = a(y1:y2,:);       % narrows the analysis on the dosimeter columns
a = double (a);                % doubles precision
for n=1:alt
```

```
c = a (n,x1:x2);                    % narrows the analysis on the dosimeter rows
m= max(c);                          % creates a matrix with each row's maximum
                                          % value (GL) and its two adjacent values
ind = find (c==max (c));
x_max = x1+ind;
e(n,1:3)=a(n,(x_max-1):(x_max+1));
end

aa = imread (location2);     % repeats the same operations with the second
                                            % photo
aa(1:alt,:) = aa(y1:y2,:);
aa = double (aa);
for n=1:alt
c = aa (n,x1:x2);
m= max(c);
ind = find (c==max (c));
x_max = x1+ind;
ee(n,1:3)=aa(n,(x_max-1):(x_max+1));
end

for n=1:alt              % calculates the mean ODD value for each row
    for i=3
    eelog(i)=log10(e(n,i)/ee(n,i));
    end
    meanvalue=mean(eelog);
    singlerow(n)=meanvalue;
end
ODD(nn)=mean(singlerow);     % calculates the average dosimeter's ODD
end
ODD                                       % prints on screen the ODD values
```

This second software is an evolution of the first designed to give ODD profiles, and it works with one dosimeter at a time.

```
function[profile]=profilosingolad(name,x1,x2,y1,y2,yd1,yd2)

% y1,y2 = matrix rows between which the dosimeter is located before
                % irradiation
```

```
% yd1,yd2 = matrix rows between which the dosimeter is located after
                % irradiation. This complication was necessary due to mismatches ir
                % photos
alt= y2-y1+1;

location = strcat ('C:\Users\raff\Desktop\tesi\Rez 2012\Cannucce in
                            cuvette\cu',name,'\1p.bmp');
location2 = strcat ('C:\Users\raff\Desktop\tesi\Rez 2012\Cannucce in
                            cuvette\cu',name,'\1d.bmp');

    a = imread (location);

a(1:alt,:) = a(y1:y2,:);
a = double (a);
for n=1:alt
d = x1:x2;
c = a (n,x1:x2);
m= max(c);
ind = find (c==max (c));
x_max = x1+ind;
e(n,1:3)=a(n,(x_max-1):(x_max+1));
end

aa = imread (location2);
aa(1:alt,:) = aa(yd1:yd2,:);
aa = double (aa);
for n=1:alt
c = aa (n,x1:x2);
m= max(c);
ind = find (c==max (c));
x_max = x1+ind;
ee(n,1:3)=aa(n,(x_max-1):(x_max+1));
end


for n=1:alt
    for i=3
    eelog(i)=log10(e(n,i)/ee(n,i));
    end
```

```
    meanvalue=mean(eelog);
    profile(n,1)=media;
end

profilo     % prints the profile vector on the screen
filename = strcat('profile_',name,'.xls');    % creates an Excel file with the pro
save (nomefile,'profilo','-ascii');
ODD=mean(profile);   %calculates and prints the average dosimeter's ODD
ODD
```

Bibliography

[1] R. F. Barth, J. A. Coderre, M. Graça H. Vicente, et al.
Boron Neutron Capture Therapy of Cancer: Current Status and Future Prospects.
Clinical Cancer Research, 2005

[2] International Atomic Energy Agency
Current status of neutron capture therapy.
IAEA, Vienna, 2001

[3] *Recommendations for the Dosimetry of Boron Neutron Capture Therapy(BNCT).*
NRG, Petten, 2003

[4] International Commission on Radiation Units and Measurements
Conversion Coefficients for use in Radiological Protection against External Radiation (Report 57)
ICRU, 1998

[5] G. Gambarini, S. Agosteo, P. Marchesi, E. Nava, P. Palazzi, A. Pecci, G. Rosi, R. Tinti
emphDiscriminations of Various Contributions to the Absorbed Dose in BNCT: Fricke-gel Imaging and Intercomparison with other Experimental Results
App. Rad. Isot. 53, 765-772, 2000.

[6] G. Gambarini, G. Bartesaghi, M. Carrara, A. Negri, L. Paganini, E. Vanossi, J. Burian, M. Marek, L. Viererbl, V. Klupak, J. Rejchrt

Imaging of Gamma and Neutron Dose Distributions at LVR-15 Epithermal Beam by means of FGLDs App. Rad. Isot. 69, 1911-1914, 2011

[7] J. Kysela
Experimental Research Reactor LVR-15 present status and programs
Nuclear Research Institute Rez, plc., Czeck Republic

[8] J. Kysela, J. Ernest, M. Marek
LVR-15 Reactor Performance and Transformation to low enriched Fuel
Nuclear Research Institute Rez, plc., Czeck Republic

[9] J. Burian, M. Marek, J. Rataj, S. Flibor, J. Rejchrt, L. Viererbl, F. Sus, H. Honova, L. Petruzelka, K. Prokes, F. Tovarys, V. Dbaly, V. Benes, P. Kozler, J. Honzatko, I. Tomandl, V. Mares, J. Marek, M. Syrucek
Report on the First Patient Group of the Phase I BNCT Trial at the LVR-15 Reactor
"Research and Development in Neutron Capture Therapy" (Sauerwein, Moss, Witting editors), Proceedings of 10th Int. Congress on NCT for Cancer, Essen, Germany, September 2002

[10] J. Burian, V. Klupak, M. Marek, J. Rejchrt, L. Viererbl, G. Gambarini, G. Bartesaghi
LVR-15 Reactor Epithermal Neutron Beam Parameters - Results of Measurements
App. Rad. Isot. 67, S202-S205, 2009

[11] J. Burian, S. Flibor, M. Marek, J. Rejchrt, L. Viererbl, I. Tomandl
Physics for BNCT
Journal of Physics: Conference Series **41**, 174-186, 2006.

[12] G. Gambarini, C. Birattari, M. Mariani, R. Marchesini, L. Pirola, P. Prestini, M. Sella, S. Tomatis
Study of Light Transmittance from Layers of Fricke-Xylenol-Orange-Gel Dosimeters
Nucl. Instr. and Meth. (B 213, 321-324), 2004

[13] A. Appleby, A. Leghrouz
Imaging of Radiation Dose by Visible Colour Development in Ferrous Agarose Xylenol Orange Gel
Med. Phys. 18 309-12, 1991

[14] G. Gambarini, M. Carrara, S. Gay, S. Tomatis
Dose Imaging with Gel-Dosimeter Layers: Optical Analysis and Dedicated Software
Radiation Protection Dosimetry, 2006

[15] G. Gambarini, V. Collia, S. Gaya, C. Petrovich, L. Pirola, G. Rosi
In-phantom Imaging of all Dose Components in Boron Neutron Capture Therapy by means of Gel Dosimeters
App. Rad. Isot. 61(5), 759-73, 2004

[16] T. Matzumoto, O. Aizawa
Depth-dose Evaluation ond Optimization of the Irradiation Facility for Boron Neutron Capture Therapy of Brain Tumours
Phys. Med. Biol., 30[9], 1985

[17] G. Bartesaghi, J. Burian, G. Gambarini, M. Marek, A. Negri, L. Viererbl
Evaluation of all Dose Components in the LVR-15 Reactor Epithermal Neutron Beam using Fricke Gel Dosimeter Layers App. Rad. Isot. 67, S199-S201, 2009